Embedded Vehicle Dynamics and LASER Aiding Techniques for Inertial Navigation Systems

J.F. Vasconcelos*, C. Silvestre†, P. Oliveira‡

Instituto Superior Técnico, Institute for Systems and Robotics, Lisbon, Portugal

This work evaluates the impact of two state-of-the-art aiding techniques to enhance the performance of inertial navigation systems (INS). A new embedded methodology to integrate the vehicle dynamics (VD) in the navigation system is proposed, by modeling it directly in the Extended Kalman Filter. The embedded VD and the INS algorithm propagate simultaneously the inertial states, allowing for the estimation of the INS errors by exploiting the dynamical information enclosed in the vehicle model. Results show that the attitude, velocity and inertial sensors bias estimates are enhanced by the comprehensive number of states predicted by the VD. The proposed technique introduces computational savings, with an accuracy equivalent to the classical external vehicle model implementations. A LASER range finder sensor is also introduced as an external aiding source and integrated into the navigation system to provide high precision altitude readings for the critical takeoff and landing maneuvers. The paper shows that the proposed technique represents a step towards the use of Uninhabited Air Vehicles in mission scenarios with limited GPS availability and/or high accuracy positioning requirements. The performance of the INS aiding architecture is assessed in simulation, and results obtained with the full nonlinear dynamics of a model-scale helicopter are presented and discussed.

Nomenclature

Notation

$\bar{\mathbf{s}}$	Nominal vector
$\mathbf{s}_r$	Sensor measurement of vector $\bar{\mathbf{s}}$
$\mathbf{s}$	Compensated vector
$\hat{\mathbf{s}}$	Estimated vector
$\delta\mathbf{s} = \mathbf{s} - \bar{\mathbf{s}}$	Vector error
$[\mathbf{s}\times]$	Cross product operator for vector $\mathbf{s}$
$\|\mathbf{s}\|$	Magnitude of vector $\mathbf{s}$
${}^F\mathbf{s}$	Vector expressed in coordinate frame $\{F\}$
$\mathbf{A}'$	Transpose of matrix $\mathbf{A}$
$f\|_{\mathbf{x}_0}$	Function $f(\mathbf{x})$ evaluated at point $\mathbf{x}_0$
$:=$	Quantity is defined as
$\equiv$	Quantity is equivalent to

Symbols

$\{E\}, \{B\}$	Earth and body coordinate frames
${}^B\mathbf{a}_{SF}$	Specific force expressed in body frame
$\mathbf{a}, \mathbf{v}, \mathbf{p}$	Acceleration, velocity, and position expressed in Earth frame
$\boldsymbol{\omega}, \mathbf{u}$	Body angular rate and linear velocity expressed in body frame
$\mathbf{b}_a, \mathbf{b}_\omega$	Accelerometer and rate gyro triads biases expressed in body frame

*PhD Student, Institute for Systems and Robotics (ISR), Instituto Superior Técnico (IST), Av. Rovisco Pais, 1, Torre Norte, 8° Andar, 1049-001, Lisboa, Portugal, AIAA Member. E-mail: jfvasconcelos@isr.ist.utl.pt

†Assistant Professor, ISR, IST, AIAA Member. E-mail: cjs@isr.ist.utl.pt

‡Assistant Professor, ISR, IST. E-mail: pjcro@isr.ist.utl.pt

$\mathbf{g}$, $\mathbf{m}$	Earth gravitational and magnetic fields
$\mathbf{n}_a, \mathbf{n}_\omega, \mathbf{n}_m$	Accelerometer, rate gyro, and magnetometer triads zero mean Gaussian white noises with variances $\sigma_a^2, \sigma_\omega^2, \sigma_m^2$ respectively
$\boldsymbol{\lambda}$	Rotation vector with magnitude $\lambda = \|\boldsymbol{\lambda}\|$
${}^E_B\mathbf{R}(\boldsymbol{\lambda})$	Rotation matrix from body to Earth coordinate frames, parametrized by $\boldsymbol{\lambda}$
$\mathcal{R}$	Shorthand notation for ${}^E_B\mathbf{R}(\boldsymbol{\lambda})$
$\mathbf{I}_{n\times n}, \mathbf{0}_{n\times n}$	n-dimensional identity and zeros matrices ($\mathbf{I} \equiv \mathbf{I}_{3\times 3}$ and $\mathbf{0} \equiv \mathbf{0}_{3\times 3}$)

Subscripts and Superscripts

k	Time index
$-, +$	Predicted and updated filter states

I. Introduction

The latest technological developments bring about Uninhabited Air Vehicles (UAVs) as versatile, multi-purpose platforms able to perform a wide variety of missions. The vast scope of practical applications ranges from coastal surveillance, bridge monitoring, traffic watch, to domestic security and search and rescue missions in extreme environments.

In particular, model-scale helicopters step forward as a challenging platform with the ability to perform Vertical Takeoff and Landing (VTOL), featuring high maneuverability and complex, fast open-loop unstable dynamics. For extended time enduring missions, these vehicles require ultra light weight, high performance, robust low cost navigation systems.

Low cost inertial navigation systems limitations, associated to open-loop unbounded estimation errors, are tackled by introducing additional data sources. Information obtained from aiding sensor suites or vehicle modeling is integrated using filtering techniques to yield accurate attitude and position estimates. Interestingly enough, the vehicle model dynamics aiding provides a comprehensive number of state estimates to compensate for the inertial errors, bearing performance improvements on most state variables. Given the fact that vehicle model dynamics is a software based solution, available in virtually any operating scenario, the scientific community has drawn its attention towards this specific aiding source.

This paper focuses on the role of vehicle dynamics (VD) aiding techniques for low cost navigation systems, and presents a new method to introduce the vehicle model in the inertial navigation system (INS). The proposed architecture is based on computing the vehicle dynamics using the INS state estimates, exploiting the redundancy of the VD and the INS algorithms information. Whereas previous work on integrating full state vehicle information involved the additional estimation and compensation of the vehicle model errors, the new method integrates the VD directly in the Extended Kalman Filter (EKF) to estimate exclusively the INS errors. The main benefits are the associated computational savings and the ability to easily select which VD equations within the full state vehicle model are implemented. Simulation results for a full actuated rigid body and for a Vario X-Treme helicopter dynamic model show that the new vehicle model aiding technique effectively enhances the navigation system results, tackling the inertial sensor's bias calibration errors. Also, the LASER range finder sensor implementation for takeoff and landing operations is detailed, enhancing the vertical channel position and velocity estimates. The VD and LASER aiding techniques provide a valuable navigation aiding solution for mission scenarios with limited GPS availability and/or with high accuracy requirements.

The dead-reckoning INS algorithm computes attitude, velocity and position based on the inertial sensor readings. Global attitude high precision INS algorithms that account for high frequency attitude, velocity and position motions (denoted as coning, sculling and scrolling respectively) are developed in Refs. 1–4. The inertial exact attitude, velocity and position computations are affected by inertial sensor biases and noise. In recent vehicle literature Refs. 5–11, the EKF is adopted to dynamically compensate for non-ideal sensor characteristics that otherwise yield unbounded INS errors.

Classical GPS/INS navigation strategies involving inertial sensor biases estimation are found to hold only partial observability for a time-invariant configuration, as discussed in Refs. 7, 12, 13. Whereas the INS computations are generic and do not reflect the VD specific information, the vehicle model is a software based aiding technique that introduces unique vehicle data to tackle state observability limitations. Also, generic aiding sensors can be subject to interference and jamming, whereas the vehicle model is a passive

information source valid for most operating conditions.

Simple motion constraints have been successfully implemented in the past for land vehicle applications, by introducing the concept of virtual observations, see Refs. 6, 8, 10. Nonholonomic constraints of wheeled vehicles, namely the inability to takeoff or perform lateral translation, are exploited in the navigation system by inputting zero valued virtual measurements of the body frame y and z axes velocity. Also, vehicle dynamics bandwidth information and frequency contents are successfully implemented to trace inertial motion and tackle bias misalignment errors in Ref. 5.

Full state, complex aircraft dynamics have been adopted to enhance the observability of the navigation system in recent work, see Refs. 6, 11. The navigation system structure is composed by a VD block that plays the role of an extra INS unit. More precisely, the vehicle dynamics are computed by a vehicle model simulator and the output is compared to the INS state estimates. The EKF state model is augmented to dynamically estimate both the INS and the VD errors. It is shown that the EKF successfully compensates for the errors in the INS and VD algorithms, improving the overall navigation system accuracy.

A convincing discussion about the impact of process model complexity on the improvement of the navigation system performance is presented in Ref. 14. Simple vehicle model is shown to clearly tackle state uncertainty and that small improvements in the VD model are more relevant to the performance enhancement than the choice of aiding sensor suites. A drawback in more complex dynamics lies in the modeling errors, overparametrization of the model, and poor observability of the vehicle states, which bias and degrade the filter performance, and that must be compensated in the form of state model uncertainty and/or using weak constraints. Although very complex models may contain unobservable modes, from the navigation system viewpoint it may only be necessary that a valid combination of the states is observable.[11]

The proposed navigation system architecture is presented in Figure 1. The framework is composed by an INS/EKF architecture. The INS is a multirate, high precision algorithm that computes attitude, velocity and position using the data from the inertial sensors. These sensors readings are affected by non-ideal errors, such as bias and noise, that degrade the INS estimates. The EKF compares the aiding sensor and vehicle model information with the INS output, under the form of a measurement residual, and compensates for the estimated inertial unit errors using a direct feedback configuration.

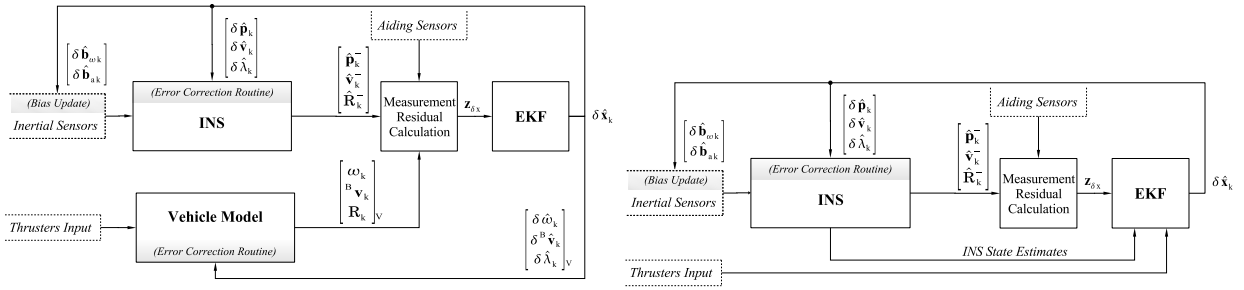

(a) External Vehicle Dynamics

(b) Internal Vehicle Dynamics

Figure 1. Navigation system block diagram

In the first architecture, shown in Figure 1(a), the vehicle dynamics are computed by an external VD simulator based on the available thrusters input information. The distinct nature of the error sources and system dynamics[11] allows the EKF to separate the INS errors from the VD errors and to perform their mutual updating in the compensation routines. Recalling the fundamentals of filtering and sensor fusion, the VD and INS ensemble is expected to yield better performance than any of the systems independently. It is worth noticing that the accuracy of the INS is increased at the cost of integrating the VD model and states, augmenting the EKF states to compensate for the VD model errors, and using error compensation routines in the external vehicle model.

In the second architecture, that is the main contribution of the present paper, the VD information is directly merged in the EKF state model, as depicted in Figure 1(b), using the INS states to compute the VD dynamics. In this setup, the inertial state estimates are integrated by both the INS and the VD equations over a sampling interval, and the VD algorithm output are described as a function of the INS errors. The distinct VD and INS integration methods applied to the same inertial quantity enables the EKF to estimate and compensate for the inertial errors. Unlike classical VD aiding, this technique avoids the use of correction routines for the VD states.

The proposed technique reduces the computational load associated to the VD model error estimation and compensation, and is especially suited for low cost hardware. Also, the vehicle dynamics are implemented incrementally in the EKF, using the same analytical results derived for the VD error estimation of the first architecture. Because INS states are used in the VD computations, vehicle model equations are partially decoupled and it is possible to select only those dynamics that are more exact.

The derived vehicle aiding techniques are introduced and validated using a generic fully actuated rigid body simulator, and extended to a model-scale Vario X-Treme helicopter model simulator, to demonstrate its application to realistic setups.

This paper is organized as follows. Section II describes the main aspects of the navigation system. Section III presents the vehicle model characteristics and the vehicle model aiding architectures. Two alternative methods to introduce the vehicle information in the navigation system are detailed and the associated computational complexity is discussed. Section IV characterizes the LASER sensor and describes the integration of the sensor information into the navigation system structure. Section V provides implementation details of the simulation setup. The VD and LASER range finder sensor based navigation systems are simulated for standard UAV maneuvers and results are discussed in Section VI. Finally, Section VII draws concluding remarks and comments on future work.

II. Navigation System Structure

In a standalone INS, inertial sensor errors compensation is usually performed offline. Even so, unbounded INS errors arise over time due to the effects of noise integration, sensor misalignment and bias calibration errors. The EKF dynamically estimates, compensates and bounds the INS errors using aiding data sources, see Figure 1. This Section presents a brief summary on the main characteristics of the INS and EKF algorithms adopted in this work. Namely the concept of multirate high accuracy inertial algorithm, the EKF error state space formulation and the error compensation routines are introduced. This overview is intended to provide the necessary background to integrate the LASER and the VD model on the navigation system. For further details on the navigation system, see Ref. 5 and references therein.

A. Inertial Navigation System

The INS performs attitude, velocity and position numerical integration from rate gyro and accelerometer triads data, rigidly mounted on the vehicle structure (strapdown configuration). For highly maneuverable vehicles, the INS numerical integration must properly address the fast dynamics of inertial sensors output, to avoid estimation errors buildup. The INS algorithm adopted in this paper is found detailed on the tutorial work presented in Ref. 1,2,4. Angular, velocity and position high frequency motions, referred to as coning, sculling, and scrolling respectively, are properly accounted for using a multirate, recursive approach. In this framework, a high speed, low order algorithm computes dynamic angular rate/acceleration effects at a small sampling interval, and its output is periodically fed to a moderate-speed algorithm that computes attitude/velocity resorting to exact, closed-form equations.

The moderate-speed inertial algorithms attitude output is represented in Direction Cosine Matrix (DCM) form, $\mathcal{R}$, and velocity and position are expressed in Earth frame coordinates, $\mathbf{v}$ and $\mathbf{p}$ respectively. A standard low-power consumption DSP based hardware architecture is found sufficient to run the algorithm at the highest accuracy repetition rates. Therefore, for a low cost setup, high computational precision is obtained and the INS error sources restrict to inertial sensor bias and noise.

B. Extended Kalman Filter

To estimate and compensate for the inertial errors, classical EKF algorithm[15] compares the INS output with the aiding sensor data. The EKF error equations, based on perturbational rigid body kinematics, were brought to full detail by Britting.[16] In particular, the attitude error $\delta\boldsymbol{\lambda}$ is parametrized by an unconstrained rotation vector representation in Earth coordinates, which can be assumed locally linear and non-singular.[17] For equivalent attitude parametrization, see Refs. 17, 18. Given the rotation error matrix definition[16] $\mathcal{R}(\delta\boldsymbol{\lambda}) := \mathcal{R}\bar{\mathcal{R}}'$, the attitude error rotation vector $\delta\boldsymbol{\lambda}$ is described by the first order approximation

$$\mathcal{R}(\delta\boldsymbol{\lambda}) \simeq \mathbf{I}_{3\times3} + [\delta\boldsymbol{\lambda}\times] \Rightarrow [\delta\boldsymbol{\lambda}\times] \simeq \mathcal{R}\bar{\mathcal{R}}' - \mathbf{I}_{3\times3} \tag{1}$$

The attitude, velocity, and position error dynamics, as well as inertial sensor's bias estimation errors, are given by

$$\begin{aligned}
\delta\dot{\mathbf{p}} &= \delta\mathbf{v} \\
\delta\dot{\mathbf{v}} &= -\mathcal{R}\delta\mathbf{b}_a - [\mathcal{R}^B\mathbf{a}_{SF}\times]\delta\boldsymbol{\lambda} + \mathcal{R}\mathbf{n}_a \\
\delta\dot{\boldsymbol{\lambda}} &= -\mathcal{R}\delta\mathbf{b}_\omega + \mathcal{R}\mathbf{n}_\omega \\
\delta\dot{\mathbf{b}}_a &= -\mathbf{n}_{b_a} \\
\delta\dot{\mathbf{b}}_\omega &= -\mathbf{n}_{b_\omega}
\end{aligned} \tag{2}$$

where ${}^B\mathbf{a}_{SF} = {}^B\mathbf{a} + {}^B\mathbf{g}$, $\mathbf{n}_{b_a}$, $\mathbf{n}_{b_\omega}$ are zero mean Gaussian white noises, and the inertial sensors biases are modeled as random walk processes, $\dot{\mathbf{b}}_a = \mathbf{n}_{b_a}, \dot{\mathbf{b}}_\omega = \mathbf{n}_{b_\omega}$.

The error compensation routines are specific to the INS algorithms and error state space representations. In the current direct feedback configuration, the EKF error estimates are compensated in the INS moderate-speed algorithm, using

$$\begin{aligned}
\mathbf{p}_k^+ &= \mathbf{p}_k^- - \delta\hat{\mathbf{p}}_k \\
\mathbf{v}_k^+ &= \mathbf{v}_k^- - \delta\hat{\mathbf{v}}_k \\
\mathcal{R}_k^+ &= \mathcal{R}'_k(\delta\hat{\boldsymbol{\lambda}}_k)\mathcal{R}_k^- \\
\mathbf{b}_{a\,k}^+ &= \mathbf{b}_{a\,k} - \delta\hat{\mathbf{b}}_{a\,k} \\
\mathbf{b}_{\omega\,k}^+ &= \mathbf{b}_{\omega\,k}^- - \delta\hat{\mathbf{b}}_{\omega\,k}
\end{aligned} \tag{3}$$

where matrix $\mathcal{R}'_k(\delta\hat{\boldsymbol{\lambda}}_k)$ is implemented using power series expansion of trigonometric terms up to an arbitrary accuracy.[19] The EKF error estimates are reset after being applied to compensate the INS states, thus updating the linearization point and keeping filter perturbational dynamics valid under the first order assumptions.

III. Vehicle Model Aiding

Classical GPS/INS architectures involving inertial sensor biases estimation are found to hold only partial observability for time-invariant configurations.[7,12,13] The vehicle dynamics arise as an inexpensive, software based solution to overcome the lack of observability in the navigation system. Given the thrusters input, the vehicle model provides redundant angular and linear velocities estimates. By handing the VD output information to the EKF, linear and angular velocities observability is enhanced. Moreover, although position is unobservable from the vehicle dynamics,[6] the velocity accuracy improvements are expected to reduce position estimation errors variance.

This Section presents the VD model and the architecture to integrate the VD information in the navigation system, depicted in Figure 1, is introduced and detailed. In particular, a new methodology to directly embed the vehicle information in the EKF is presented.

The external VD structure, depicted in Figure 1(a), follows from previous work found in Refs. 6, 11. Vehicle state estimates are computed by a vehicle simulator block, using the thrusters input information. The full state vehicle model algorithm computes attitude and velocity estimates that are compared to the INS output, under the form of measurement residuals. Whereas the vehicle aiding information is expected to help the INS, computational and modeling errors of the vehicle dynamics itself must be addressed by the filter. Therefore, the EKF state model is also augmented to compensate for the vehicle modeling errors.

The current work presents a new, alternative method to exploit the VD model by blending the vehicle simulator equations directly in the EKF state model. Vehicle dynamics are integrated in the filter state space, linearized about the inertial state estimates. The vehicle dynamics propagate the inertial estimates, so the VD integration is a function of the INS errors. Therefore, the EKF algorithm internally solves the VD equations and only outputs the INS error estimates, as shown in Figure 1(b).

A. Body Dynamics

To illustrate the VD aiding technique proposed in this paper, the straightforward dynamics of a rigid body are first adopted, corresponding to a 6-DOF polyhedron with uniform mass density and fully actuated. After

validating in simulation the derived internal VD navigation system, the same technique is then tested on the Vario X-Treme helicopter dynamics model detailed in Appendix A.

The Body coordinate frame origin, denoted $\mathbf{p}_{Borg}$, is located at the body's center of mass and geometric center. The axes of the Body frame define a plane of symmetry for the mass distribution of the body, so the resulting body inertia tensor, denoted $\mathbf{I}_B$, is described by the principal moments of inertia,[20] yielding

$$\mathbf{I}_B = \frac{m}{12}\begin{bmatrix} h^2+l^2 & 0 & 0 \\ 0 & w^2+h^2 & 0 \\ 0 & 0 & l^2+w^2 \end{bmatrix} \tag{4}$$

where m is the body mass and (l, w, h) represent the polyhedron length, width and height, respectively. The rigid body is subject to the thrusters force and momentum, denoted $\mathbf{f}_{th}$ and $\mathbf{n}_{th}$ respectively, and to viscous linear and angular damping, denoted ${}^B\mathbf{f}_d$ and ${}^B\mathbf{n}_d$ respectively, yielding

$$\begin{array}{ll} \mathbf{f}_{th} = \sum_i \mathbf{f}_i, & \mathbf{n}_{th} = \sum_i {}^B\mathbf{p}_{th\,i} \times \mathbf{f}_i \\ {}^B\mathbf{f}_d = -K_{lin}{}^B\mathbf{v}, & {}^B\mathbf{n}_d = -K_{ang}\boldsymbol{\omega} \end{array} \tag{5}$$

where $i = 1 \ldots 6$ denotes the thruster's index that applies force $\mathbf{f}_i$ to the body, ${}^B\mathbf{p}_{th\,i}$ are the thrusters' coordinates in Body frame, and K_{lin} and K_{ang} are the linear and angular damping coefficients respectively.

Applying the Newton and Euler equations to determine body's translation and rotation with respect to the inertial frame, the body dynamics are expressed by the nonlinear state space model

$$\dot{\bar{\boldsymbol{\omega}}}_V := \quad f_\omega(\bar{\boldsymbol{\omega}}_V, \bar{\mathbf{n}}_{th}) \quad = -\mathbf{I}_B^{-1}\left([\bar{\boldsymbol{\omega}}_V\times]\,\mathbf{I}_B\bar{\boldsymbol{\omega}}_V + K_{ang}\bar{\boldsymbol{\omega}}_V\right) + \mathbf{I}_B^{-1}\bar{\mathbf{n}}_{th} \tag{6}$$

$$\dot{\bar{\mathbf{u}}}_V := \quad f_u(\bar{\boldsymbol{\omega}}_V, \bar{\mathbf{u}}_V, \bar{\mathbf{f}}_{th}) \quad = -\mathbf{M}_T^{-1}\left([\bar{\boldsymbol{\omega}}_V\times]\,\mathbf{M}_T\bar{\mathbf{u}}_V + K_{lin}\bar{\mathbf{u}}_V\right) + \mathbf{M}_T^{-1}\bar{\mathbf{f}}_{th} + \bar{\mathcal{R}}'_V{}^E\mathbf{g} \tag{7}$$

$$\dot{\bar{\mathcal{R}}}_V := \quad f_{\mathcal{R}}(\bar{\boldsymbol{\omega}}_V, \bar{\mathcal{R}}_V) \quad = \bar{\mathcal{R}}_V\,[\bar{\boldsymbol{\omega}}_V\times] \tag{8}$$

where the Body and the Center of Mass coordinate frames, denoted $\{B\}$ and $\{G\}$ respectively, are defined with the same orientation and position, so the body frame attitude dynamics (6) do not depend on the linear velocity.

The V subscript for the angular velocity and body linear velocity (6-8) is adopted to emphasize that these quantities are computed using the vehicle dynamics. As mentioned is Section II.A, these quantities are also computed by the INS, using distinct inertial algorithms. The correspondence between the VD and INS quantities is straightforward, $\boldsymbol{\omega}_V \equiv \boldsymbol{\omega}$ and $\mathbf{u}_V \equiv \mathcal{R}'\mathbf{v}$, whereas the nominal quantities are exactly equal, $\bar{\boldsymbol{\omega}}_V = \bar{\boldsymbol{\omega}}$ and $\bar{\mathbf{u}}_V = \bar{\mathcal{R}}'\bar{\mathbf{v}}$. For simulation purposes, the rigid body dynamics yield physical intuition on the contribution of the vehicle model to the inertial states errors observability and compensation.

B. External Vehicle Model Aiding

In the classical VD aiding, presented in Figure 1(a), the vehicle dynamics are computed using a standalone vehicle simulator, appended to the navigation system and external to the EKF/INS system. The EKF state model is augmented to estimate and compensate for the VD block errors, using particular error compensation routines.

The VD block error dynamics are formulated using the same technique adopted to describe the INS error dynamics.[5] These are obtained by applying a perturbational analysis to the nominal dynamics (6-8). Let $\mathbf{x}_V = (\boldsymbol{\omega}_V, \mathbf{u}_V, \mathcal{R}_V)$ denote the vehicle states, the vehicle model error dynamics are described by the first order terms of the Taylor series expansion

$$\dot{\boldsymbol{\omega}}_V = f_\omega(\boldsymbol{\omega}_V, \mathbf{n}_{th}) \Rightarrow \dot{\delta\boldsymbol{\omega}}_V \approx \left.\frac{\partial f_\omega}{\partial \boldsymbol{\omega}}\right|_{\mathbf{x}_V}\delta\boldsymbol{\omega}_V + \left.\frac{\partial f_\omega}{\partial \mathbf{n}_{th}}\right|_{\mathbf{x}_V}\delta\mathbf{n}_{th} \tag{9}$$

$$\dot{\mathbf{u}}_V = f_u(\boldsymbol{\omega}_V, \mathbf{u}_V, \mathcal{R}_V, \mathbf{f}_{th}) \Rightarrow \dot{\delta\mathbf{u}}_V \approx \left.\frac{\partial f_u}{\partial \boldsymbol{\omega}}\right|_{\mathbf{x}_V}\delta\boldsymbol{\omega}_V + \left.\frac{\partial f_u}{\partial \mathbf{u}}\right|_{\mathbf{x}_V}\delta\mathbf{u}_V + \left.\frac{\partial f_u}{\partial \delta\boldsymbol{\lambda}}\right|_{\mathbf{x}_V}\delta\boldsymbol{\lambda}_V + \left.\frac{\partial f_u}{\partial \mathbf{f}_{th}}\right|_{\mathbf{x}_V}\delta\mathbf{f}_{th} \tag{10}$$

where the Jacobians are given by

$$\left.\frac{\partial f_\omega}{\partial \boldsymbol{\omega}}\right|_{\mathbf{x}_V} = \mathbf{I}_B^{-1}\left(\left[\mathbf{I}_B\boldsymbol{\omega}_V\times\right] - \left[\boldsymbol{\omega}_V\times\right]\mathbf{I}_B - \mathbf{I}\,K_{ang}\right), \qquad \left.\frac{\partial f_\omega}{\partial \mathbf{n}_{th}}\right|_{\mathbf{x}_V} = \mathbf{I}_B^{-1}$$
$$\left.\frac{\partial f_u}{\partial \boldsymbol{\omega}}\right|_{\mathbf{x}_V} = \mathbf{M}_T^{-1}\left[\mathbf{M}_T\mathbf{u}_V\times\right], \qquad \left.\frac{\partial f_u}{\partial \mathbf{u}}\right|_{\mathbf{x}_V} = \mathbf{M}_T^{-1}\left(-\left[\boldsymbol{\omega}_V\times\right]\mathbf{M}_T - \mathbf{I}\,K_{lin}\right) \tag{11}$$
$$\left.\frac{\partial f_u}{\partial \delta\boldsymbol{\lambda}}\right|_{\mathbf{x}_V} = \mathcal{R}_V'\left[{}^E\mathbf{g}\times\right], \qquad \left.\frac{\partial f_u}{\partial \mathbf{f}_{th}}\right|_{\mathbf{x}_V} = \mathbf{M}_T^{-1}$$

The rotation matrix dynamics (8) are described by the inertial rigid body kinematics, so the associated error dynamics are identical to the INS attitude error (2), yielding $\delta\dot{\boldsymbol{\lambda}}_V = \mathcal{R}_V\delta\boldsymbol{\omega}_V$.

The INS and VD state estimates are compared under the form of measurement residuals, obtained by the perturbational method applied in Ref. 5 and described by

$$\begin{aligned}
\delta\mathbf{z}_\omega &:= \boldsymbol{\omega} - \boldsymbol{\omega}_V = \bar{\boldsymbol{\omega}} + \delta\boldsymbol{\omega} - (\bar{\boldsymbol{\omega}} + \delta\boldsymbol{\omega}_V) = \delta\boldsymbol{\omega} - \delta\boldsymbol{\omega}_V \\
&= -\delta\mathbf{b}_\omega - \delta\boldsymbol{\omega}_V + \mathbf{n}_\omega \\
\delta\mathbf{z}_u &:= \mathcal{R}'\mathbf{v} - \mathbf{u}_V = \mathcal{R}'\mathbf{v} - ({}^B\bar{\mathbf{v}} + \delta\mathbf{u}_V) \\
&= (\mathcal{R}' - \bar{\mathcal{R}}')\mathbf{v} + \bar{\mathcal{R}}'\delta\mathbf{v} - \delta\mathbf{u}_V = -\mathcal{R}'\left[\boldsymbol{\lambda}\times\right]\mathbf{v} + \bar{\mathcal{R}}'\delta\mathbf{v} - \delta\mathbf{u}_V \\
&\approx \mathcal{R}'\delta\mathbf{v} + \mathcal{R}'\left[\mathbf{v}\times\right]\delta\boldsymbol{\lambda} - \delta\mathbf{u}_V \\
\delta\mathbf{z}_{\boldsymbol{\lambda}} &:= \mathcal{R}\mathcal{R}_V' - \mathbf{I} \approx \left[\mathbf{I} + \left[\delta\boldsymbol{\lambda}\times\right]\right]\bar{\mathcal{R}}\bar{\mathcal{R}}'\left[\mathbf{I} - \left[\delta\boldsymbol{\lambda}_V\times\right]\right] - \mathbf{I} \\
&\approx \delta\boldsymbol{\lambda} - \delta\boldsymbol{\lambda}_V
\end{aligned} \tag{12}$$

where the rate gyro errors are defined by $\delta\boldsymbol{\omega} = -\delta\mathbf{b}_\omega + \mathbf{n}_\omega$.

The vehicle model equations (6-8) are computed by a variable-step Runge-Kutta differential equation solver, using the known thrusters force $\mathbf{f}_{th}$ and momentum $\mathbf{n}_{th}$. The vehicle state errors and covariances are propagated by the EKF using the (9-11) dynamics and assuming that the thrusters input is known, $\delta\mathbf{n}_{th} = \delta\mathbf{f}_{th} = \mathbf{0}_{3\times1}$. Actual implementation of the navigation system may require that the thrusters errors be parametrized by stochastic uncertainties.

The INS and VD error estimates are updated with the measurement residuals (12) and compensated in the external vehicle simulator, as shown in Figure 1(a), using the following error compensation routines

$$\begin{aligned}
\boldsymbol{\omega}_{V\,k}^+ &= \boldsymbol{\omega}_{V\,k}^- - \delta\hat{\boldsymbol{\omega}}_{V\,k} \\
\mathbf{u}_{V\,k}^+ &= \mathbf{u}_{V\,k}^- - \delta\hat{\mathbf{u}}_{V\,k} \\
\mathcal{R}_{V\,k}^+ &= \mathcal{R}_{V\,k}'(\delta\hat{\boldsymbol{\lambda}}_V)\mathcal{R}_{V\,k}^-
\end{aligned} \tag{13}$$

similar to the INS error compensation routines (3).

C. Internal Vehicle Model Aiding

In the external VD aiding architecture, the vehicle dynamics are computed by a standalone algorithm, and the EKF state model (2) is augmented to estimate the VD error dynamics (6-8). The INS and the VD states dynamics are uncorrelated, and their observation is based on measuring a linear combination (12) of the INS and the VD errors. In the external VD aiding methodology, computational resources are allocated to estimate and compensate for the VD errors, as a mean to estimate and compensate for the INS errors.

A new method to implement the VD aiding is motivated by the idea of replacing the vehicle inertial states, such as $\boldsymbol{\omega}_V$, $\mathbf{u}_V$ and $\mathcal{R}_V$, by the INS estimates, respectively $\boldsymbol{\omega}$, $\mathcal{R}'\mathbf{v}$ and $\mathcal{R}$, and propagating the inertial quantities through the vehicle dynamics. The VD results are described as a function of the INS errors, allowing the EKF to estimate and compensate for the inertial errors. This way, error estimation and compensation routines are only performed in the INS, reducing the computational cost associated to VD aiding techniques.

The new method also allows to select which vehicle dynamics are adopted, in the case some modeled dynamics are more precise than others, allowing for the use of those that yield better accuracy. For example, VD velocity (7) can be computed using the INS attitude estimate $\mathcal{R}$ instead of computing the vehicle attitude $\mathcal{R}_V$ dynamics (8), or the navigation system can be aided by using only VD angular velocity dynamics (6) without computing the linear velocity dynamics (7) if these are inaccurate.

Let $\mathbf{x} = (\boldsymbol{\omega}, \mathbf{v}, \mathcal{R})$ denote the INS state estimates. In the internal VD methodology, nominal vehicle dynamics (6-7) are linearized about the INS state estimates. Using the first order terms of the Taylor series expansion yields

$$\dot{\bar{\boldsymbol{\omega}}}_V = \quad f_\omega(\bar{\boldsymbol{\omega}}, \bar{\mathbf{n}}_{th}) \quad \approx f_\omega(\boldsymbol{\omega}, \mathbf{n}_{th}) + \left.\frac{\partial f_\omega}{\partial \boldsymbol{\omega}}\right|_{\mathbf{x}} (\bar{\boldsymbol{\omega}} - \boldsymbol{\omega}) + \left.\frac{\partial f_\omega}{\partial \mathbf{n}_{th}}\right|_{\mathbf{x}} (\bar{\mathbf{n}}_{th} - \mathbf{n}_{th}) \tag{14}$$

$$\begin{aligned}\dot{\bar{\mathbf{u}}}_V = \quad f_u(\bar{\boldsymbol{\omega}}, \bar{\mathbf{u}}, \bar{\mathcal{R}}, \bar{\mathbf{f}}_{th}) \quad &\approx f_u(\boldsymbol{\omega}, \mathbf{u}, \mathcal{R}, \mathbf{f}_{th}) + \left.\frac{\partial f_u}{\partial \boldsymbol{\omega}}\right|_{\mathbf{x}} (\bar{\boldsymbol{\omega}} - \boldsymbol{\omega}) + \left.\frac{\partial f_u}{\partial \mathbf{u}}\right|_{\mathbf{x}} (\bar{\mathbf{u}} - \mathbf{u}) + \left.\frac{\partial f_u}{\partial \delta\boldsymbol{\lambda}}\right|_{\mathbf{x}} \delta\boldsymbol{\lambda} \\ &\quad + \left.\frac{\partial f_u}{\partial \mathbf{f}_{th}}\right|_{\mathbf{x}} (\bar{\mathbf{f}}_{th} - \mathbf{f}_{th})\end{aligned} \tag{15}$$

The INS estimate error is defined as the difference between the nominal state and the INS estimate. Therefore, the nominal angular and linear velocities are expressed as a function of the INS states and estimation errors by

$$\begin{aligned}\dot{\bar{\boldsymbol{\omega}}}_V &\approx f_\omega(\boldsymbol{\omega}, \mathbf{n}_{th}) - \left.\frac{\partial f_\omega}{\partial \boldsymbol{\omega}}\right|_{\mathbf{x}} \delta\boldsymbol{\omega} - \left.\frac{\partial f_\omega}{\partial \mathbf{n}_{th}}\right|_{\mathbf{x}} \delta\mathbf{n}_{th} \\ &= f_\omega(\boldsymbol{\omega}, \mathbf{n}_{th}) + \left.\frac{\partial f_\omega}{\partial \boldsymbol{\omega}}\right|_{\mathbf{x}} \delta\mathbf{b}_\omega - \left.\frac{\partial f_\omega}{\partial \boldsymbol{\omega}}\right|_{\mathbf{x}} \mathbf{n}_\omega - \left.\frac{\partial f_\omega}{\partial \mathbf{n}_{th}}\right|_{\mathbf{x}} \delta\mathbf{n}_{th}\end{aligned} \tag{16}$$

$$\begin{aligned}\dot{\bar{\mathbf{u}}}_V &\approx f_u(\boldsymbol{\omega}, \mathbf{u}, \mathcal{R}, \mathbf{f}_{th}) - \left.\frac{\partial f_u}{\partial \boldsymbol{\omega}}\right|_{\mathbf{x}} \delta\boldsymbol{\omega} - \left.\frac{\partial f_u}{\partial \mathbf{u}}\right|_{\mathbf{x}} \delta\mathbf{u} - \left.\frac{\partial f_u}{\partial \delta\boldsymbol{\lambda}}\right|_{\mathbf{x}} \delta\boldsymbol{\lambda} - \left.\frac{\partial f_u}{\partial \mathbf{n}_{th}}\right|_{\mathbf{x}} \delta\mathbf{n}_{th} - \left.\frac{\partial f_u}{\partial \mathbf{f}_{th}}\right|_{\mathbf{x}} \delta\mathbf{f}_{th} \\ &= f_u(\boldsymbol{\omega}, \mathbf{u}, \mathcal{R}, \mathbf{f}_{th}) - \left.\frac{\partial f_u}{\partial \mathbf{u}}\right|_{\mathbf{x}} \mathcal{R}'\delta\mathbf{v} - \left(\left.\frac{\partial f_u}{\partial \delta\boldsymbol{\lambda}}\right|_{\mathbf{x}} + \left.\frac{\partial f_u}{\partial \mathbf{u}}\right|_{\mathbf{x}} \mathcal{R}' \left[\mathbf{v}\times\right]\right) \delta\boldsymbol{\lambda} + \left.\frac{\partial f_u}{\partial \boldsymbol{\omega}}\right|_{\mathbf{x}} \delta\mathbf{b}_\omega \\ &\quad - \left.\frac{\partial f_u}{\partial \boldsymbol{\omega}}\right|_{\mathbf{x}} \mathbf{n}_\omega - \left.\frac{\partial f_u}{\partial \mathbf{n}_{th}}\right|_{\mathbf{x}} \delta\mathbf{n}_{th} - \left.\frac{\partial f_u}{\partial \mathbf{f}_{th}}\right|_{\mathbf{x}} \delta\mathbf{f}_{th}\end{aligned} \tag{17}$$

where body linear velocity error $\delta\mathbf{u}$ is rewritten as a function of the INS state errors $\delta\mathbf{u} := \mathcal{R}'\mathbf{v} - \bar{\mathcal{R}}'\bar{\mathbf{v}} \approx \mathcal{R}' \left[\mathbf{v}\times\right] \delta\boldsymbol{\lambda} + \mathcal{R}'\delta\mathbf{v}$.

Equations (16-17) describe the nominal angular and linear dynamics as the result of solving the vehicle dynamics $f_\omega(\boldsymbol{\omega}, \mathbf{n}_{th})$ and $f_u(\boldsymbol{\omega}, \mathbf{u}, \mathcal{R}, \mathbf{f}_{th})$ using the INS states, and correcting the first order effects of the INS errors in the vehicle dynamics using the linearization Jacobians. Interestingly enough, the vehicle dynamics functions applied to the inertial estimates do not yield the INS state estimate derivatives, $\dot{\boldsymbol{\omega}} \neq f_\omega(\boldsymbol{\omega}, \mathbf{n}_{th}), \dot{\mathbf{u}} \neq f_u(\boldsymbol{\omega}, \mathbf{u}, \mathcal{R}, \mathbf{f}_{th})$, which is a clear consequence of the distinct, compatible models enclosed in the VD and INS computations. The thrusters input is considered to be known, $\delta\mathbf{n}_{th} = \delta\mathbf{f}_{th} = \mathbf{0}_{3\times1}$.

The navigation system observations are drawn directly from the INS inertial estimates

$$\begin{aligned}\mathbf{z}_\omega &:= \boldsymbol{\omega} = \bar{\boldsymbol{\omega}} - \delta\mathbf{b}_\omega + \mathbf{n}_\omega \\ \mathbf{z}_u &:= \mathcal{R}'\mathbf{v} = \bar{\mathcal{R}}' \left(\mathbf{I} - \left[\delta\boldsymbol{\lambda}\times\right]\right) \bar{\mathbf{v}} + \mathcal{R}'\delta\mathbf{v} \\ &\approx \bar{\mathbf{u}} + \mathcal{R}'\delta\mathbf{v} + \mathcal{R}' \left[\mathbf{v}\times\right] \delta\boldsymbol{\lambda}\end{aligned} \tag{18}$$

The proposed technique is designed using the Jacobians computed for the classical method (11). Hence, the analytical results needed to integrate the vehicle model in the EKF are the same for both architectures. On the other hand, the number of states is reduced, because the INS information is directly used in the vehicle dynamics, which reduces the computational cost associated to the introduction of vehicle dynamics in the Kalman filter. The VD error compensation routines (13) are not necessary in this technique.

IV. LASER Aiding

In this Section, the LASER range finder aiding sensor is described and the corresponding filter observation equation is introduced. Without loss of generality, the sensor is assumed to be mounted along the z axis of the frame $\{M\}$, whose relative orientation to the body frame is described by the known installation rotation matrix ${}^B_M\mathbf{R}$. The LASER reads the distance L from the vehicle to the ground, along the z axis of the $\{M\}$ coordinate frame, as depicted in Figure 2. The high accuracy of the LASER sensor is especially suited for landing and takeoff operations of an air vehicle. Other changeling applications for the LASER sensor are the relative positioning of the vehicle with respect to a structure.

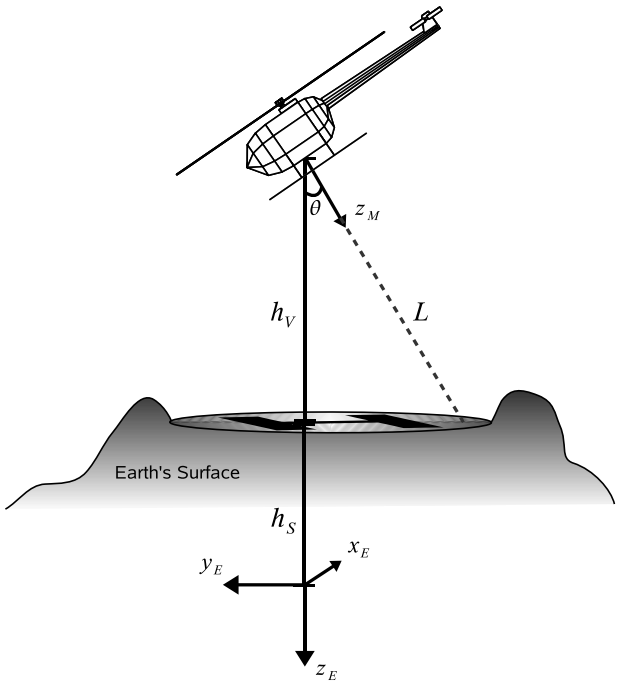

Figure 2. LASER Range Finder Reading

In the current work, the landing area terrain is assumed to be locally planar, such as an heliport or a landing lane. The Earth's surface height $\bar{h}_S$, given by the distance from the Earth frame origin to the Earth surface, is modeled as approximately constant

$$\dot{\bar{h}}_S = n_{h_S} \tag{19}$$

where n_{h_S} is a zero mean Gaussian white noise process whose variance reflects the uncertainty on the ground's flatness.

Let $\bar{\mathbf{p}} = (\bar{p}_x, \bar{p}_y, \bar{p}_z)$ be vehicle position coordinates in the Earth frame. As depicted in Figure 2, the z axis Earth coordinate of the vehicle is given by

$$\bar{p}_z = -(\bar{h}_S + \bar{h}_V) \tag{20}$$

where $\bar{h}_V \geq 0$ is the vehicle's height, that is, the distance from Body frame origin to the Earth surface.

Using elementary trigonometric relations yields

$$\cos(\theta) = \frac{\bar{h}_V}{\bar{L}} = \frac{|{}^M\bar{\mathbf{h}}'_V \mathbf{e}_z|}{|{}^E\bar{\mathbf{h}}'_V \mathbf{e}_z|} \tag{21}$$

where ${}^E\bar{\mathbf{h}}_V = (0, 0, -\bar{h}_V)$ is the vehicle's height in Earth coordinates, $\mathbf{e}_z = (0, 0, 1)$ is the unitary z axis vector and ${}^M\bar{\mathbf{h}}'_V \mathbf{e}_z$ corresponds to the projection of $\bar{\mathbf{h}}_V$ on the z axis of the $\{M\}$ frame.

Applying the coordinate transform ${}^M\bar{\mathbf{h}}_V = (\bar{\mathcal{R}}\,{}^B_M\bar{\mathbf{R}})'\,{}^E\bar{\mathbf{h}}_V$ and developing the terms in the previous equation, the LASER range is described by

$$\bar{L} = \frac{\bar{h}_V}{\mathbf{e}'_z \bar{\mathcal{R}}^B_M \bar{\mathbf{R}} \mathbf{e}_z} \tag{22}$$

where $\bar{L}$ is not defined for the cases where the LASER is pointing upwards, that is $\mathbf{e}'_z \bar{\mathcal{R}}^B_M \bar{\mathbf{R}} \mathbf{e}_z \leq 0$.

The LASER range finder sensor measures the actual range $\bar{L}$ corrupted by the sensor noise

$$L_r = \bar{L} + \delta L \tag{23}$$

where $\delta L = n_L$ is modeled as a zero mean Gaussian white noise with variance σ_L^2.

The LASER sensor is used primarily to perform landing maneuvers, providing high accuracy estimates of the vehicle distance to the ground along the $\{M\}$ coordinate frame z axis. The measurement residual is computed by

$$\delta \mathbf{z}_L \quad := \quad p_z - (-h_V) \tag{24}$$

where the height estimate from the LASER reading is given by rearranging the terms in (22)

$$h_V = \mathbf{e}_z' \mathcal{R}_M^B \bar{\mathbf{R}} \mathbf{e}_z L_r \tag{25}$$

and the INS position estimate

$$p_z = \bar{p}_z + \delta p_z = -\bar{h}_S - \bar{h}_V + \mathbf{e}_z' \delta \mathbf{p} \tag{26}$$

that includes the summation of the vehicle's and Earth's surface heights, $\bar{h}_S$ and $\bar{h}_V$ respectively, which are filtered apart by modeling the h_S dynamics (19) in the EKF.

Replacing the INS attitude estimate $\mathcal{R}$ by the attitude error $\delta \boldsymbol{\lambda}$ approximation (1) and neglecting second order terms yields

$$\begin{aligned} \bar{h}_V &= \mathbf{e}_z' \bar{\mathcal{R}}_M^B \bar{\mathbf{R}} \mathbf{e}_z \bar{L} \approx \mathbf{e}_z' \left[\mathbf{I}_{3\times 3} - [\delta \boldsymbol{\lambda} \times] \right] \mathcal{R}_M^B \bar{\mathbf{R}} \mathbf{e}_z \bar{L} \\ &\approx \mathbf{e}_z' \mathcal{R}_M^B \bar{\mathbf{R}} \mathbf{e}_z (L_r - \delta L) + L_r \mathbf{e}_z' \left[\mathcal{R}_M^B \bar{\mathbf{R}} \mathbf{e}_z \times \right] \delta \boldsymbol{\lambda} \\ &= h_V - \mathbf{e}_z' \mathcal{R}_M^B \bar{\mathbf{R}} \mathbf{e}_z \delta L + \mathbf{e}_z' \left[\mathcal{R}_M^B \bar{\mathbf{R}} \mathbf{e}_z \times \right] \delta \boldsymbol{\lambda} \end{aligned} \tag{27}$$

From equations (23-27), the measurement residual is described as a function of the EKF state variables

$$\delta \mathbf{z}_L = \mathbf{e}_z' \delta \mathbf{p} - \mathbf{e}_z' \left[\mathcal{R}_M^B \bar{\mathbf{R}} \mathbf{e}_z \times \right] \delta \boldsymbol{\lambda} - \bar{h}_S + \mathbf{e}_z' \mathcal{R}_M^B \bar{\mathbf{R}} \mathbf{e}_z \mathbf{n}_L \tag{28}$$

For practical applications, the landing and takeoff locations have different terrain height h_S. After the takeoff and during flight operations, the LASER sensor is switched off to prevent erroneous readings due to the terrain height fluctuations and to the interference of obstacles located between the vehicle and the ground. When the landing maneuver starts, the LASER is switched on to estimate the new h_S. A method to estimate h_S using the filter uncertainty is discussed in Section V and validated in Section VI.

V. Implementation

In this Section, the state space model matrices for the VD aiding architectures and LASER sensor integration in the INS/EKF navigation system are detailed. The state variables and measurement residuals associated to the VD dynamics are cast in the state model formulation, evidencing the differences between the external and internal vehicle model aiding techniques. The computational savings obtained by using the internal vehicle model aiding are detailed. Discrete-time equivalent of the continuous state space model is deduced for implementation purposes.

The standard formulation for the continuous-time state space dynamics is described by

$$\dot{\mathbf{x}}_C = \mathbf{F}_C \left(\mathbf{x}_C \right) \mathbf{x}_C + \mathbf{G}_C \left(\mathbf{x}_C \right) \mathbf{n}_{x_C} + \mathbf{u}_C \tag{29}$$

$$\mathbf{z} = \mathbf{H}_C \left(\mathbf{x}_C \right) \mathbf{x}_C + \mathbf{n}_{z_C} \tag{30}$$

where $\mathbf{x}_C$ is the state vector, $\mathbf{F}_C$ is the state dynamics matrix, $\mathbf{n}_{x_C}$ is the state noise transformed by matrix $\mathbf{G}_C$, $\mathbf{u}_C$ is the system input vector, and $\mathbf{z}$ is the state measurement, corrupted by the noise vector $\mathbf{n}_{z_C}$. The state and measurement noises are assumed zero mean, Gaussian white noises with covariance matrices denoted by $\mathbf{Q}_C$ and $\mathbf{R}_C$, respectively.

A. INS/EKF state model

The state error estimates dynamics are immediate from the inertial errors model (2). Let $\mathbf{x}_{\text{INS}} = \left(\mathbf{p}, \mathbf{v}, \mathcal{R}, {}^{B}\mathbf{a}_{SF}, \boldsymbol{\omega}\right)$ denote the inertial estimates, the INS/EKF architecture state dynamics are described by

$$\begin{aligned}
\hat{\mathbf{x}}_C \equiv \delta\hat{\mathbf{x}} &= \begin{bmatrix} \delta\hat{\mathbf{p}}' & \delta\hat{\mathbf{v}}' & \delta\hat{\boldsymbol{\lambda}}' & \delta\hat{\mathbf{b}}_a' & \delta\hat{\mathbf{b}}_\omega' \end{bmatrix}', \\
\mathbf{F}_C(\mathbf{x}_{\text{INS}}) \equiv \mathbf{F}_{\text{INS}} &= \begin{bmatrix} \mathbf{0} & \mathbf{I} & \mathbf{0} & \mathbf{0} & \mathbf{0} \\ \mathbf{0} & \mathbf{0} & -\left[\mathcal{R}\,{}^{B}\mathbf{a}_{SF}\times\right] & -\mathcal{R} & \mathbf{0} \\ \mathbf{0} & \mathbf{0} & \mathbf{0} & \mathbf{0} & -\mathcal{R} \\ \mathbf{0} & \mathbf{0} & \mathbf{0} & \mathbf{0} & \mathbf{0} \\ \mathbf{0} & \mathbf{0} & \mathbf{0} & \mathbf{0} & \mathbf{0} \end{bmatrix} \\
\mathbf{n}_{x_C} \equiv \mathbf{n}_{\text{INS}} &= \begin{bmatrix} \mathbf{n}_p' & \mathbf{n}_a' & \mathbf{n}_\omega' & \mathbf{n}_{b_a}' & \mathbf{n}_{b_\omega}' \end{bmatrix}', \quad \mathbf{u}_C \equiv \mathbf{0} \\
\mathbf{G}_C(\mathbf{x}_{\text{INS}}) \equiv \mathbf{G}_{\text{INS}} &= \texttt{blkdiag}\left(\mathbf{I}, \mathcal{R}, \mathcal{R}, -\mathbf{I}, -\mathbf{I}\right)
\end{aligned} \tag{31}$$

where $\texttt{blkdiag}(...)$ represents a block diagonal matrix, $\mathbf{n}_p$ is a fictitious zero mean Gaussian white noise associated to the position error estimate and the state noise covariance matrix is given by

$$\mathbf{Q}_C \equiv \mathbf{Q}_{\text{INS}} = \texttt{blkdiag}(\sigma_p^2\mathbf{I}, \sigma_a^2\mathbf{I}, \sigma_\omega^2\mathbf{I}, \sigma_{b_a}^2\mathbf{I}, \sigma_{b_\omega}^2\mathbf{I}) \tag{32}$$

The measurement equations (30) are determined by the aiding techniques integrated in the navigation system. The measurement model for the proposed VD and LASER aiding techniques are described in the ensuing. For comparison purposes, a simplified GPS receiver is considered to provide position measurements corrupted by Gaussian white noise and a magnetometer aiding sensor provides Earth's magnetic field readings. The GPS and magnetometer aiding sensors are modeled in the form (30) using the measurement equations detailed in [5].

B. Vehicle Model Aiding

The EKF state space model previously described is augmented to exploit the VD and Laser dynamics and associated measurement residuals.

1. External Vehicle Model Aiding

The continuous-time error state space model for the navigation system with external VD aiding is obtained directly from the EKF/INS error state model augmented by the VD error dynamics (9-11), yielding

$$\begin{aligned}
\mathbf{x}_C &\equiv \begin{bmatrix} \delta\hat{\mathbf{x}}' & \delta\hat{\mathbf{x}}_V' \end{bmatrix}', & \mathbf{n}_{x_C} &\equiv \begin{bmatrix} \mathbf{n}_{\text{INS}}' & \mathbf{n}_{x_V}' \end{bmatrix}', & \mathbf{u}_C &\equiv \mathbf{0}, \\
\mathbf{F}_C(\mathbf{x}_{\text{INS}}, \mathbf{x}_V) &\equiv \begin{bmatrix} \mathbf{F}_{\text{INS}} & \mathbf{0}_{15\times 9} \\ \mathbf{0}_{9\times 15} & \mathbf{F}_V(\mathbf{x}_V) \end{bmatrix}, & \mathbf{G}_C(\mathbf{x}_{\text{INS}}) &\equiv \begin{bmatrix} \mathbf{G}_{\text{INS}} & \mathbf{0}_{15\times 9} \\ \mathbf{0}_{9\times 15} & \mathbf{G}_V \end{bmatrix},
\end{aligned} \tag{33}$$

with the vehicle states, noises and model submatrices given by

$$\begin{aligned}
\delta\hat{\mathbf{x}}_V &= \begin{bmatrix} \delta\hat{\boldsymbol{\omega}}_V' & \delta^{B}\hat{\mathbf{v}}_V' & \delta\hat{\boldsymbol{\lambda}}_V{}' \end{bmatrix}, & \mathbf{n}_{x_V} &= \begin{bmatrix} \mathbf{n}_{\boldsymbol{\omega}_V}' & \mathbf{n}_{{}^{B}\mathbf{v}_V}' & \mathbf{n}_{\boldsymbol{\lambda}_V}' \end{bmatrix}, \\
\mathbf{F}_V(\mathbf{x}_V) &= \begin{bmatrix} \frac{\partial f_\omega}{\partial \boldsymbol{\omega}} & \mathbf{0} & \mathbf{0} \\ \frac{\partial f_u}{\partial \boldsymbol{\omega}} & \frac{\partial f_u}{\partial \mathbf{u}} & \frac{\partial f_u}{\partial \boldsymbol{\lambda}} \\ \mathcal{R}_V & \mathbf{0} & \mathbf{0} \end{bmatrix}\Bigg|_{\mathbf{x}_V}, & \mathbf{G}_V &= \begin{bmatrix} \mathbf{I} & \mathbf{0} & \mathbf{0} \\ \mathbf{0} & \mathbf{I} & \mathbf{0} \\ \mathbf{0} & \mathbf{0} & \mathbf{I} \end{bmatrix}
\end{aligned} \tag{34}$$

where $\mathbf{n}_{x_V}$ is a vector of fictitious zero mean Gaussian white noise that characterizes the vehicle modeling errors. The external VD and INS error dynamics are independent, so the state dynamics matrix $\mathbf{F}_C$ is block diagonal.

The relation between the INS and VD states is introduced by the measurement residuals (12), which is a function of the INS and VD errors, given in the state space form by

$$\mathbf{z} \equiv \delta\mathbf{z}_V = \begin{bmatrix}\delta\mathbf{z}'_\omega & \delta\mathbf{z}'_u & \delta\mathbf{z}'_{\boldsymbol{\lambda}}\end{bmatrix}', \quad \mathbf{n}_{z_V} \equiv \begin{bmatrix}\mathbf{n}'_\omega + \mathbf{n}'_{\mathbf{z}_\omega} & \mathbf{n}'_{\mathbf{z}_u} & \mathbf{n}'_{\mathbf{z}_{\boldsymbol{\lambda}}}\end{bmatrix}'$$
$$\mathbf{H}_C(\mathbf{x}_{\text{INS}}) \equiv \begin{bmatrix}\mathbf{0} & \mathbf{0} & \mathbf{0} & \mathbf{0} & -\mathbf{I} & -\mathbf{I} & \mathbf{0} & \mathbf{0} \\ \mathbf{0} & \mathcal{R}' & \mathcal{R}'[\mathbf{v}\times] & \mathbf{0} & \mathbf{0} & \mathbf{0} & -\mathbf{I} & \mathbf{0} \\ \mathbf{0} & \mathbf{0} & \mathbf{I} & \mathbf{0} & \mathbf{0} & \mathbf{0} & \mathbf{0} & -\mathbf{I}\end{bmatrix} \tag{35}$$

where $\mathbf{n}_{z_\omega}$, $\mathbf{n}_{z_U}$ and $\mathbf{n}_{z_\lambda}$ are a fictitious zero mean Gaussian white noises associated to the $\delta\mathbf{z}_V$ observation, with covariances $\sigma^2_{z_\omega}$, $\sigma^2_{z_U}$ and $\sigma^2_{z_\lambda}$ respectively. The vehicle states and measurements noise covariance matrices are

$$\mathbf{Q}_C \equiv \text{blkdiag}(\mathbf{Q}_{\text{INS}}, \sigma^2_{\omega_V}\mathbf{I}, \sigma^2_{u_V}\mathbf{I}, \sigma^2_{\mathcal{R}_V}\mathbf{I}), \qquad \mathbf{R}_C \equiv \text{blkdiag}((\sigma^2_{z_\omega} + \sigma^2_\omega)\mathbf{I}, \sigma^2_{z_u}\mathbf{I}, \sigma^2_{z_\lambda}\mathbf{I}) \tag{36}$$

where the fictitious white noise variances reflect the effects of neglecting second order terms in the measurement residual derivation.

In particular, the observation noise of $\delta\mathbf{z}_\omega$ includes the rate gyro noise, so a state and measurement noise correlation matrix

$$\mathbf{C}_C \equiv \begin{bmatrix}\mathbf{0} & \mathbf{0} & \sigma^2_\omega\mathbf{I} & \mathbf{0} & \mathbf{0} & \mathbf{0}_{3\times9} \\ & & \mathbf{0}_{6\times15} & & & \mathbf{0}_{6\times9}\end{bmatrix}' \tag{37}$$

is introduced in the Kalman filter equations, see Refs. 5, 15 for the definition details and the discrete-time approximation.

2. Internal Vehicle Model Aiding

The continuous-time state space model is straightforward from (16-17), yielding

$$\hat{\mathbf{x}}_C \equiv \begin{bmatrix}\delta\hat{\mathbf{x}}' & \hat{\mathbf{x}}'_V\end{bmatrix}', \quad \mathbf{n}_{x_C} \equiv \begin{bmatrix}\mathbf{n}'_{\text{INS}} & \mathbf{n}'_{x_V}\end{bmatrix}', \quad \mathbf{u}_C \equiv \begin{bmatrix}f_\omega(\boldsymbol{\omega}, \mathbf{N}_{th})' & f_u(\boldsymbol{\omega}, {}^B\mathbf{v}, \mathcal{R}, \mathbf{F}_{th})'\end{bmatrix}'$$
$$\mathbf{F}_C(\mathbf{x}_{\text{INS}}) \equiv \begin{bmatrix}\mathbf{F}_{\text{INS}} & \mathbf{0}_{15\times6} \\ \mathbf{F}_V(\mathbf{x}_{\text{INS}}) & \mathbf{0}_{6\times6}\end{bmatrix}, \quad \mathbf{G}_C(\mathbf{x}_{INS}) \equiv \begin{bmatrix}\mathbf{G}_{\text{INS}} & \mathbf{0}_{9\times6} \\ \mathbf{G}_V(\mathbf{x}_{\text{INS}}) & \mathbf{I}_{6\times6}\end{bmatrix} \tag{38}$$

with the vehicle states, noises and submatrices described by

$$\hat{\mathbf{x}}_V = \begin{bmatrix}\hat{\boldsymbol{\omega}}'_V & \hat{\mathbf{u}}'\end{bmatrix}', \quad \mathbf{n}_{x_V} = \begin{bmatrix}\mathbf{n}'_{\boldsymbol{\omega}_V} & \mathbf{n}'_{\mathbf{u}_V}\end{bmatrix}',$$
$$\mathbf{F}_V(\mathbf{x}_{\text{INS}}) = \begin{bmatrix}\mathbf{0} & \mathbf{0} & \mathbf{0} & \mathbf{0} & \frac{\partial f_\omega}{\partial\boldsymbol{\omega}}, \\ \mathbf{0} & -\frac{\partial f_u}{\partial\mathbf{u}}\mathcal{R}' & -\left(\frac{\partial f_u}{\partial\delta\boldsymbol{\lambda}} + \frac{\partial f_u}{\partial\mathbf{u}}\mathcal{R}'[\mathbf{v}\times]\right) & \mathbf{0} & \frac{\partial f_u}{\partial\boldsymbol{\omega}}\end{bmatrix}\Bigg|_{\mathbf{x}_{\text{INS}}} \tag{39}$$
$$\mathbf{G}_V(\mathbf{x}_{\text{INS}}) = \begin{bmatrix}\mathbf{0} & \mathbf{0} & -\frac{\partial f_\omega}{\partial\boldsymbol{\omega}} & \mathbf{0} & \mathbf{0} \\ \mathbf{0} & \mathbf{0} & -\frac{\partial f_u}{\partial\boldsymbol{\omega}} & \mathbf{0} & \mathbf{0}\end{bmatrix}\Bigg|_{\mathbf{x}_{\text{INS}}}$$

where $\mathbf{n}_{x_V}$ is an array of fictitious zero mean Gaussian white noise that characterizes the vehicle modeling errors. Note that the vehicle states dynamics depend only on the inertial state estimates, i.e., the state matrices depend only on the $\mathbf{x}_{\text{INS}}$ variable.

The measurement state model (18) is described in the state space form by

$$\mathbf{z} \equiv \begin{bmatrix}\mathbf{z}'_\omega & \mathbf{z}'_u\end{bmatrix}', \quad \mathbf{n}_{z_V} \equiv \begin{bmatrix}\mathbf{n}'_\omega + \mathbf{n}'_{\mathbf{z}_\omega} & \mathbf{n}'_{\mathbf{z}_u}\end{bmatrix}', \quad \mathbf{H}_C(\mathbf{x}_{INS}) \equiv \begin{bmatrix}\mathbf{0} & \mathbf{0} & \mathbf{0} & \mathbf{0} & -\mathbf{I} & \mathbf{I} & \mathbf{0} \\ \mathbf{0} & \mathcal{R}' & \mathcal{R}'[\mathbf{v}\times] & \mathbf{0} & \mathbf{0} & \mathbf{0} & \mathbf{I}\end{bmatrix} \tag{40}$$

and $\mathbf{n}_{\mathbf{z}_\omega}$ and $\mathbf{n}_{\mathbf{z}_u}$ are a fictitious zero mean Gaussian white noises associated with the measurement. The vehicle states and measurements noise covariance and covariance correlation matrices are

$$\mathbf{Q}_C \equiv \text{blkdiag}(\mathbf{Q}_{\text{INS}}, \sigma^2_{\omega_V}\mathbf{I}, \sigma^2_{u_V}\mathbf{I}), \quad \mathbf{R}_C \equiv \text{blkdiag}((\sigma^2_{z_\omega} + \sigma^2_\omega)\mathbf{I}, \sigma^2_{z_u}\mathbf{I}), \quad \mathbf{C}_C \equiv \begin{bmatrix}\mathbf{0} & \mathbf{0} & \sigma^2_\omega\mathbf{I} & \mathbf{0} & \mathbf{0} & \mathbf{0}_{3\times6} \\ & & \mathbf{0}_{3\times15} & & & \mathbf{0}_{3\times6}\end{bmatrix}' \tag{41}$$

The off-diagonal block element of $\mathbf{F}_C$ evidences that the vehicle state errors are a function of solely the inertial state estimation errors. The zeros block $\mathbf{0}_{6\times6}$ diagonal element of $\mathbf{F}_C$ facilitates the matrix exponential computational in the discretization process.

In the embedded VD formulation, the vehicle dynamics propagate $\mathbf{x}_{\text{INS}}$ instead of the vehicle states, hence the EKF does not need to update the latter $\mathbf{x}_V$. Let $\mathbf{K} = [\mathbf{K}'_{\text{INS}}\ \mathbf{K}'_V]'$ be the Kalman gain matrix, where $\mathbf{K}_{\text{INS}}$ is a (15×6) gain submatrix and $\mathbf{K}_V$ is a (6×6) gain submatrix. Using the Schmidt-Kalman gain expression,[15] the navigation system computations are reduced by skipping $\mathbf{K}_V$ and $\mathbf{x}_V$ update and simply calculating the $\mathbf{K}_{\text{INS}}$ explicitly to update $\mathbf{x}_{\text{INS}}$.

C. LASER Aiding

The continuous-time state space model for the LASER sensor is immediate from (19), bearing

$$\hat{\mathbf{x}}_C \equiv \begin{bmatrix}\delta\hat{\mathbf{x}}' & h_S\end{bmatrix}', \quad \mathbf{n}_{x_C} \equiv \begin{bmatrix}\mathbf{n}'_{\text{INS}} & n_{h_S}\end{bmatrix}', \quad \mathbf{u}_C \equiv \mathbf{0} \tag{42}$$

$$\mathbf{F}_C(\mathbf{x}_{\text{INS}}) \equiv \begin{bmatrix}\mathbf{F}_{\text{INS}} & \mathbf{0}_{15\times1}\\ \mathbf{0}_{1\times15} & 0\end{bmatrix}, \quad \mathbf{G}_C(\mathbf{x}_{INS}) \equiv \begin{bmatrix}\mathbf{G}_{\text{INS}} & \mathbf{0}_{9\times1}\\ \mathbf{0}_{1\times9} & 1\end{bmatrix} \tag{43}$$

and the measurement state model, obtained from (28), is given by

$$\mathbf{z} \equiv \delta\mathbf{z}_L, \qquad \mathbf{n}_{z_C} \equiv \mathbf{n}_{z_L}, \qquad \mathbf{H}_C(\mathbf{x}_{INS}) \equiv \begin{bmatrix}\mathbf{e}'_z & \mathbf{0}_{1\times3} & -\mathbf{e}'_z\left[\mathcal{R}_M^B\bar{\mathbf{R}}\mathbf{e}_z\times\right] & \mathbf{0}_{1\times3} & \mathbf{0}_{1\times3} & -1\end{bmatrix} \tag{44}$$

where

$$\mathbf{Q}_C \equiv \text{blkdiag}(\mathbf{Q}_{\text{INS}}, \sigma^2_{h_S}), \qquad \mathbf{R}_C \equiv (\mathbf{e}'_z\mathcal{R}_M^B\bar{\mathbf{R}}\mathbf{e}_z)^2\sigma_L^2, \qquad \mathbf{C}_C \equiv \mathbf{0} \tag{45}$$

As mentioned in Section IV, the LASER sensor is adopted for takeoff and landing maneuvers and to determine the relative position to structures. When the LASER sensor is inactive, the h_S state estimate uncertainty will grow, at a rate defined by the $\sigma^2_{\dot{h}_S}$ variance. While the noise n_{h_S} defines the terrain flatness when the LASER sensor is on, n_{h_S} models the discrepancy between h_S of different sites when the LASER is off. In the current work $\sigma^2_{\dot{h}_S}$ is defined so to provide a large uncertainty between the time the LASER is deactivated (takeoff) and activated (landing), assuming that the flight time is known. Other valid approach is to define $\sigma^2_{\dot{h}_S}$ according to the vehicle horizontal velocity and the terrain's geographic profile.

Additionally, the h_S uncertainty should be bounded during flight time to avoid numerical problems, by adopting techniques such as square root filtering[15] or by simply setting $\sigma_{h_S} = 0$ if the uncertainty reaches a prespecified upper bound.

D. State Model Discretization

The discrete-time state space model is obtained using the zero order hold discretization technique

$$\mathbf{\Phi}_k = e^{\mathbf{F}_k T}, \quad \mathbf{H}_k = \mathbf{H}_C|_{t=t_k} \tag{46}$$

and the discrete-time noise covariance matrices are[5,15,21]

$$\mathbf{Q}_k \simeq [\mathbf{G}_k\mathbf{Q}_C\mathbf{G}'_k]T, \quad \mathbf{R}_k \simeq \frac{\mathbf{R}_{Ck}}{T}, \quad \mathbf{C}_k \simeq (\mathbf{I} + \frac{\mathbf{F}_k T}{2} + \frac{\mathbf{F}_k^2 T^2}{6})\mathbf{G}_k\mathbf{C}_{Ck} \tag{47}$$

where T is the sampling period, $\mathbf{F}_k = \mathbf{F}_C|_{t=t_k}$, $\mathbf{G}_k = \mathbf{G}_C|_{t=t_k}$, $\mathbf{R}_{Ck} = \mathbf{R}_C|_{t=t_k}$, $\mathbf{C}_{Ck} = \mathbf{C}_C|_{t=t_k}$and $\mathbf{\Phi}_k = \mathbf{\Phi}(t_{k+1}, t_k)$ denotes the state transition matrix.

VI. Simulation Results

This Section validates the proposed VD and LASER range finder aiding techniques in simulation. In the first simulation, the accuracy of the navigation system aided by the VD techniques is compared to a classical GPS/INS architecture. The external and internal VD aiding techniques results are analyzed to study the performance deterioration (if any) of implementing the internal VD model. Bias estimation and velocity accuracy enhancements are presented and discussed, for a standard UAV trimming trajectory.

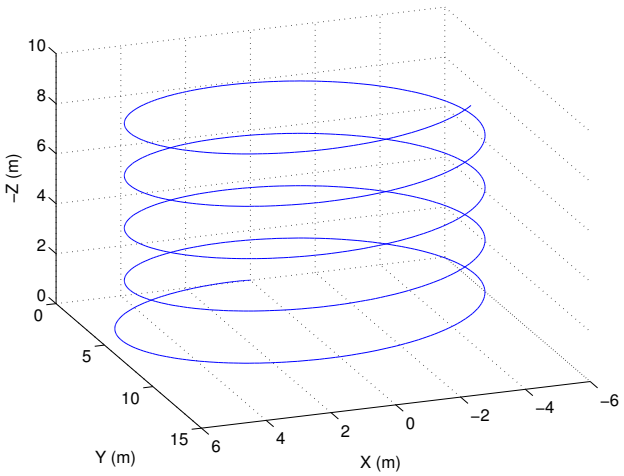

Figure 3. Trimming Trajectory

To verify the validity of using linearized models for highly nonlinear, realistic vehicle models, the proposed internal VD aiding technique is simulated on a model-scale Vario X-Treme helicopter. The model dynamics, derived from first-principles in Refs. 22,23, are summarized in Appendix A. The navigation system accuracy enhancements are illustrated and the predicted error covariance is depicted to evidence the inertial states observability improvements.

Finally, simulation are performed to show the accuracy improvements obtained with the LASER range finder sensor integrated on a GPS/INS configuration. The vehicle describes a hovering maneuver and has to acquire the ground height for a landing operation. Dynamic estimation of terrain height is performed and position and velocity vertical channel accuracy enhancements are shown.

The INS high speed algorithm is set to run at 100 Hz and the normal speed algorithm is synchronized with the EKF, both executed at 50Hz. The LASER sensor operates at 10Hz and the GPS provides position measurements at the nominal frequency of 1Hz. The vehicle model profile is detailed in Table 1 and the sensors noise and bias characteristics are presented in Table 2.

A. Vehicle Model Aiding

The rigid body is subject to constant linear and centripetal acceleration, describing the upwards trimming trajectory shown in Figure 3. To analyze the bias estimation and compensation, a $\frac{1}{3}$ bias calibration error is introduced in each channel of the accelerometer and rate gyro sensors. The external VD, embedded VD and a classical GPS/INS architecture results are presented in Figures 4 and 5 and detailed in Tables 3 and 4. Due to the poor observability of the yaw angle, see Table 3, a magnetometer aiding sensor is included.

The comprehensive number of state dynamics provided by the VD clearly endows the filter to compensate for the inertial sensor biases. Accelerometer and rate gyro biases calibration errors are quickly tackled by the VD information, yielding smaller bias estimation error variances in the VD architecture, see Figure 4.

Introducing the magnetometer aiding source improves rate gyro bias and attitude estimation, as depicted

Table 1. Rigid Body Characteristics

Property	Nominal Value
Mass	$m = 10$ Kg
Length, Width, Height	$(l, w, h) = (1.00, 0.75, 0.25)$ m
Thrusters #1 Position	${}^{B}\mathbf{p}_{th\,1,2} = (-0.50, \pm 0.30, 0)$ m
Thrusters #2 Position	${}^{B}\mathbf{p}_{th\,3,4} = (0, -0.375, \pm 0.10)$ m
Thrusters #3 Position	${}^{B}\mathbf{p}_{th\,5,6} = (\pm 0.40, 0, -0.125)$ m
Damping Coefficients	$K_{ang} = 4$, $K_{lin} = 2$

Table 2. Sensor Errors

Sensor	**Bias**	**Noise Variance** (σ^2)
Rate Gyro	0.05 °/s	$(0.02\ ^\circ/\text{s})^2$
Accelerometer	10 mg	$(0.6\ \text{mg})^2$
LASER	-	$(10^{-2}\ \text{m})^2$
Magnetometer	-	$(1\ \mu\text{G})^2$
GPS	-	$10\ \text{m}^2$

in Figure 5 and detailed in Table 3. This shows that additional aiding information can be successfully exploited in the internal VD architecture.

The accuracy improvements in position, velocity and attitude are clear from Tables 3 and 4. Although vehicle dynamics do not yield position and attitude estimates, the angular/linear velocity accuracy improvements bound the attitude/position estimation errors. Interestingly enough, due to the fast inertial bias estimation and compensation, accelerometer bias calibration errors do not yield noticeable position errors, which are effectively bounded by integrating the VD information.

The proposed internal and the external VD architectures performance results are similar. Hence, the computational savings of the internal VD aiding technique are obtained without affecting the navigation system accuracy, which validates the embedded VD approach.

Table 3. Attitude Estimation Error

Average Square Error						
	Magnetometer Off			*Magnetometer On*		
	Yaw(°)	**Pitch**(°)	**Roll**(°)	**Yaw**(°)	**Pitch**(°)	**Roll**(°)
GPS	2.99	1.88×10^{-2}	1.70×10^{-2}	1.05×10^{-8}	7.35×10^{-3}	6.65×10^{-3}
Ext. VD	1.30×10^{-2}	6.09×10^{-4}	1.39×10^{-3}	1.23×10^{-7}	2.48×10^{-4}	2.24×10^{-4}
Int. VD	2.30×10^{-2}	5.42×10^{-4}	1.47×10^{-3}	1.27×10^{-7}	3.46×10^{-4}	2.96×10^{-4}

Table 4. Position and Velocity Estimation Error (Magnetometer On)

Average Square Error						
	$\mathbf{p}_x(m)$	$\mathbf{p}_y(m)$	$\mathbf{p}_z(m)$	$\mathbf{v}_x(m/s)$	$\mathbf{v}_y(m/s)$	$\mathbf{v}_z(m/s)$
GPS	0.92	1.35	1.15	1.13×10^{-2}	3.57×10^{-2}	1.04×10^{-2}
Ext. VD	1.11×10^{-5}	1.48×10^{-2}	4.07×10^{-4}	9.57×10^{-8}	6.44×10^{-5}	1.80×10^{-7}
Int. VD	1.96×10^{-5}	2.05×10^{-2}	3.32×10^{-4}	1.46×10^{-7}	8.38×10^{-5}	2.76×10^{-7}

B. Vario X-Treme Helicopter

The rigid body simulated in the previous Section is a simple nonlinear model that allows for a physical insight on the proposed aiding techniques results, but it lacks the complexity of a realistic air vehicle. The Vario X-Treme helicopter, depicted in Figure 6, features highly nonlinear unstable dynamics and is adopted to take a step towards the implementation of the internal VD aiding technique in field applications.

The simulated takeoff trajectory, depicted in Figure 7, consists of an ascending turn, followed by a straight upwards path. As before, the $\frac{1}{3}$ bias calibration error is assumed and the magnetometer is used to compensate for the yaw observability.

Simulation results are shown in Figures 8 and 9 and detailed in Tables 5 and 6. Although the Vario X-treme model is highly nonlinear, the VD linearization technique yields accurate inertial estimates. The helicopter model aiding dramatically enhances the INS estimates, as shown in Figures 8 and 9. The filter estimated error covariance is, in general, consistent with the estimation error covariance.

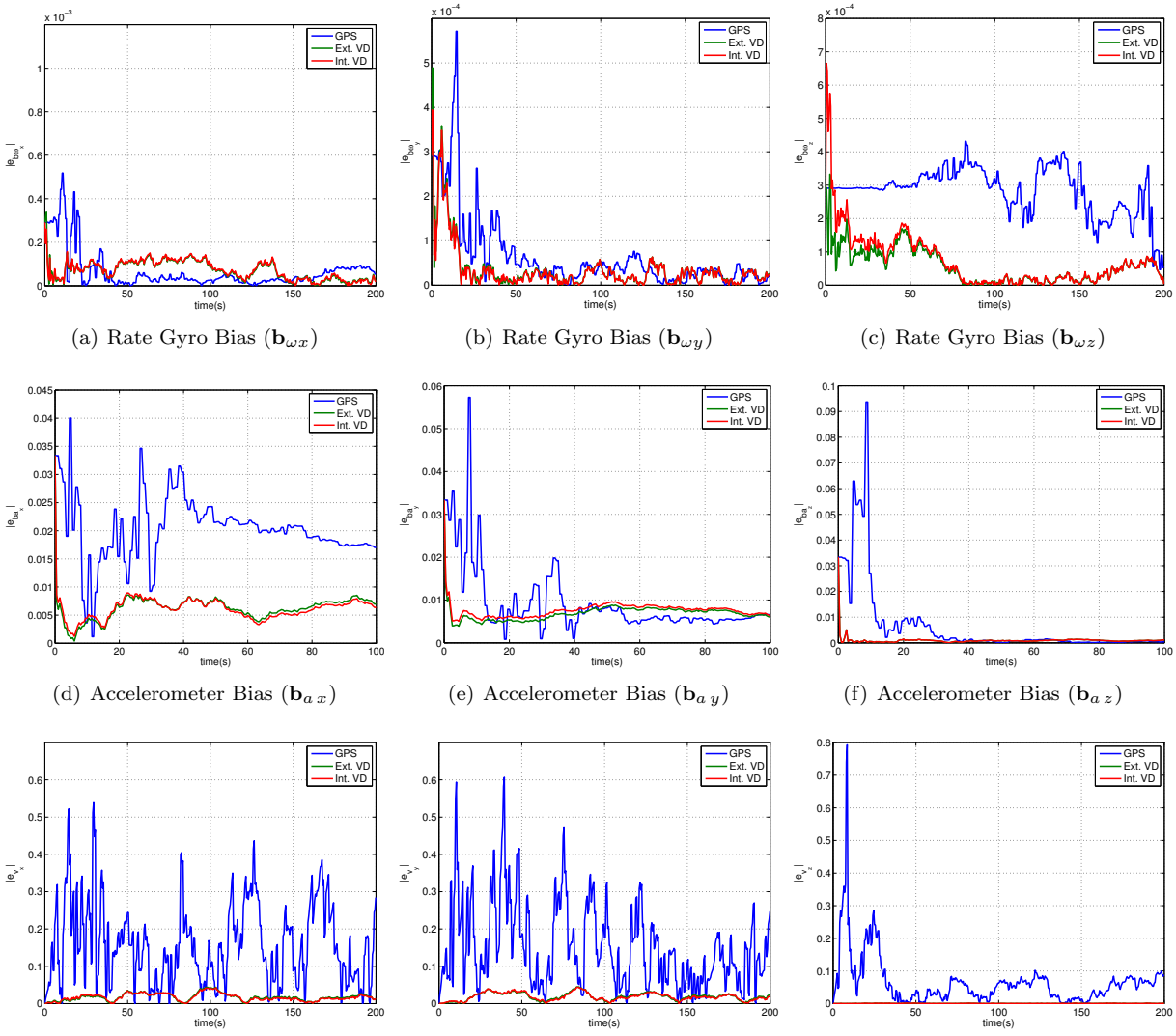

(a) Rate Gyro Bias ($\mathbf{b}_{\omega x}$) (b) Rate Gyro Bias ($\mathbf{b}_{\omega y}$) (c) Rate Gyro Bias ($\mathbf{b}_{\omega z}$)

(d) Accelerometer Bias ($\mathbf{b}_{a\,x}$) (e) Accelerometer Bias ($\mathbf{b}_{a\,y}$) (f) Accelerometer Bias ($\mathbf{b}_{a\,z}$)

(g) Velocity ($\mathbf{v}_x$) (h) Velocity ($\mathbf{v}_y$) (i) Velocity ($\mathbf{v}_z$)

Figure 4. GPS and VD Navigation Systems Estimation Errors (Magnetometer Off)

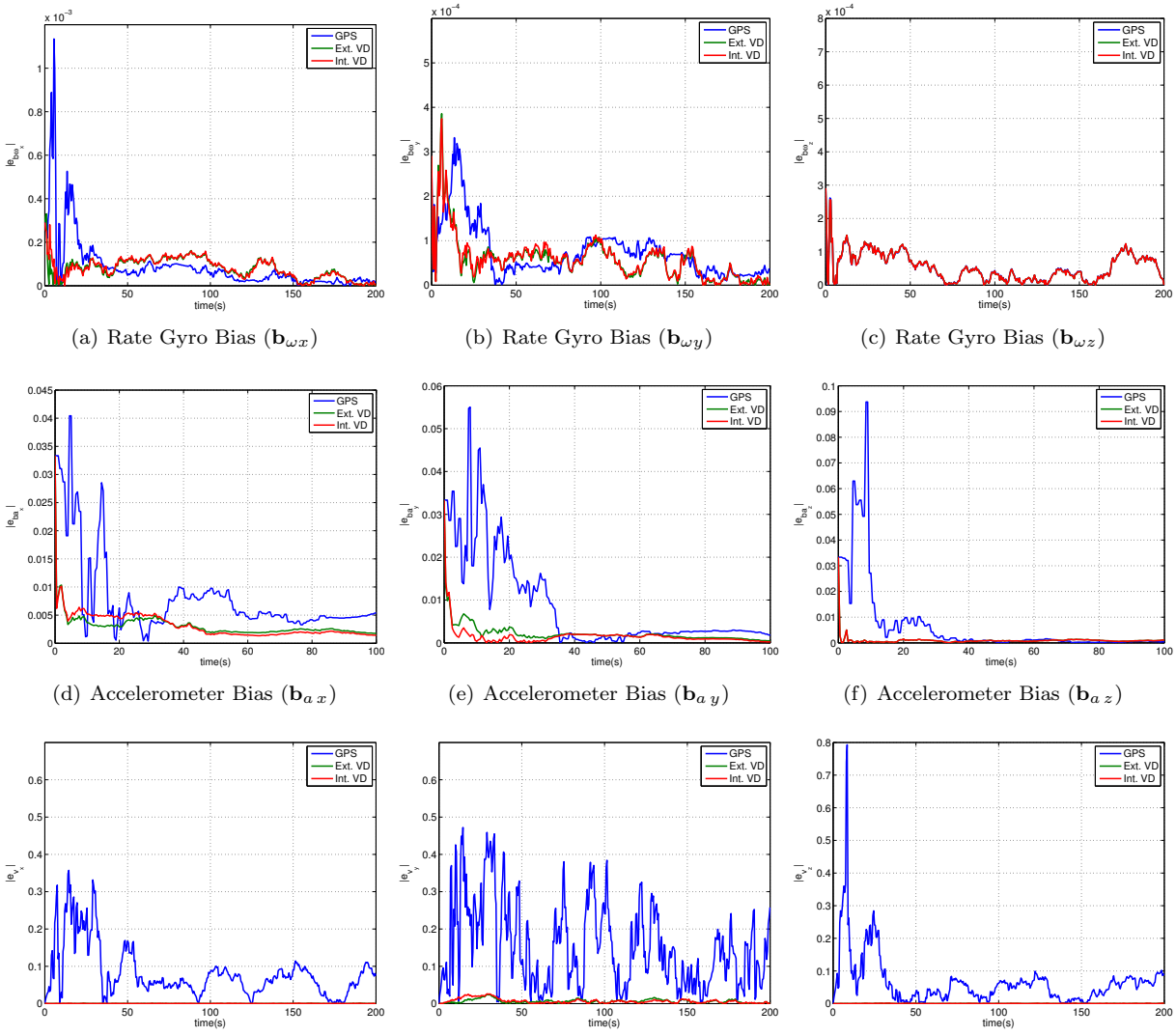

(a) Rate Gyro Bias ($\mathbf{b}_{\omega x}$) (b) Rate Gyro Bias ($\mathbf{b}_{\omega y}$) (c) Rate Gyro Bias ($\mathbf{b}_{\omega z}$)

(d) Accelerometer Bias ($\mathbf{b}_{a\,x}$) (e) Accelerometer Bias ($\mathbf{b}_{a\,y}$) (f) Accelerometer Bias ($\mathbf{b}_{a\,z}$)

(g) Velocity ($\mathbf{v}_x$) (h) Velocity ($\mathbf{v}_y$) (i) Velocity ($\mathbf{v}_z$)

Figure 5. GPS and VD Navigation Systems Estimation Errors (Magnetometer On)

Figure 6. Vario X-Treme Model-Scale Helicopter

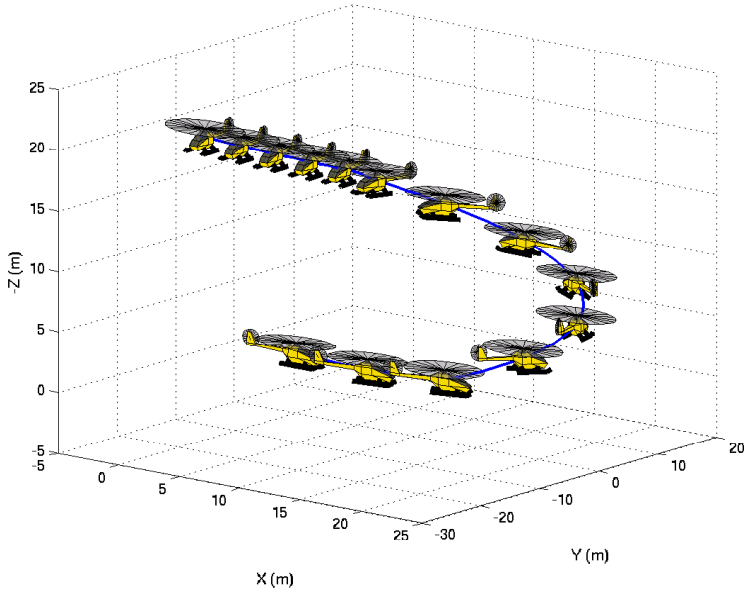

Figure 7. Vario X-Treme Simulated Trajectory

Figure 9 indicates that the VD aiding technique effectively enhances the trajectory estimation to a centimeter accuracy. As discussed in Refs. 11,14, these exciting results must be addressed with care. Vehicle modeling errors, model simplification assumptions or unmodeled time-varying parameters, perturbations and dynamics, such as vehicle load and wind gusts, may severely affect the navigation system performance if not correctly accounted for in the filter.[11]

The tuning of the noise covariance matrices, the estimation of additional states and parameters and the use of more accurate vehicle model dynamics, among other techniques,[14] are adopted to allow for the use of VD in real navigation systems. Nonetheless, side effects such as the poor observability of the augmented states, the overparametrization of the vehicle model or even the inability to obtain a vehicle model which yields information on the real vehicle dynamics may occur. The use of the full VD model in filtering is a time-consuming process, requiring navigation systems engineering expertise for complex vehicles.

On the other hand, previous work by the authors[5] has shown that using a general bandwidth description of the vehicle dynamics frequency contents yields noticeable accuracy improvements. Either using a generic or a complex vehicle model, the integration of the vehicle dynamics in the navigation system is a valuable aiding technique, especially suited for the cases of GPS outage or jamming and when other external sensors are not available or provide poor observability of the vehicle states.

Table 5. Attitude Estimation Error

Average Square Error			
	Yaw(°)	**Pitch**(°)	**Roll**(°)
GPS	1.63×10^{-7}	9.66×10^{-3}	7.33×10^{-3}
Vario X-Treme Model	7.22×10^{-9}	3.35×10^{-4}	1.66×10^{-4}

Table 6. Position and Velocity Estimation Error

Average Square Error						
	$\mathbf{p}_x(m)$	$\mathbf{p}_y(m)$	$\mathbf{p}_z(m)$	$\mathbf{v}_x(m/s)$	$\mathbf{v}_y(m/s)$	$\mathbf{v}_z(m/s)$
GPS	1.33	2.12	2.41	1.58×10^{-2}	6.76×10^{-2}	4.07×10^{-2}
Vario X-Treme Model	4.92×10^{-2}	4.71×10^{-3}	3.36×10^{-2}	7.91×10^{-4}	1.65×10^{-2}	7.51×10^{-6}

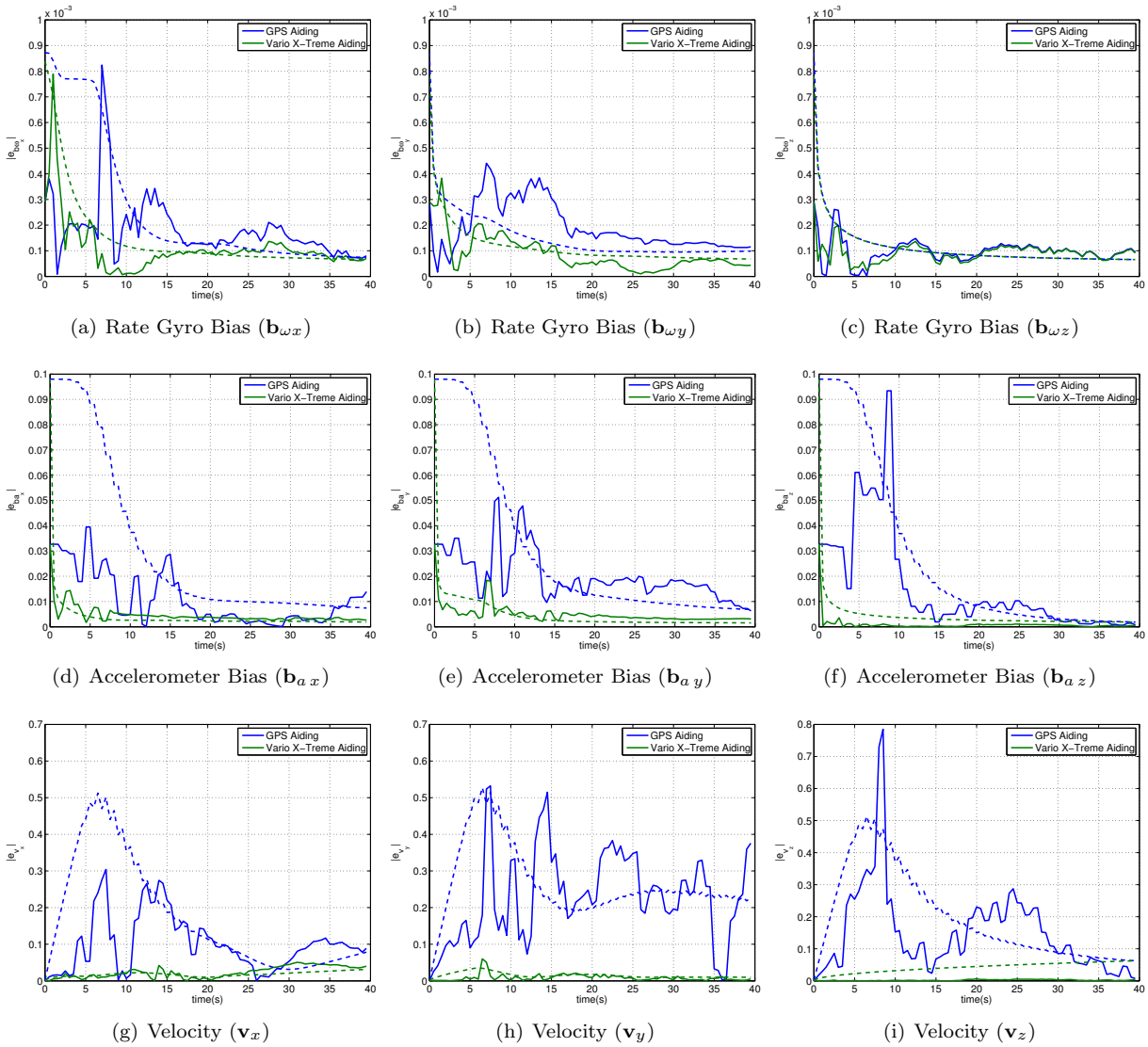

(a) Rate Gyro Bias ($\mathbf{b}_{\omega x}$) (b) Rate Gyro Bias ($\mathbf{b}_{\omega y}$) (c) Rate Gyro Bias ($\mathbf{b}_{\omega z}$)

(d) Accelerometer Bias ($\mathbf{b}_{a\,x}$) (e) Accelerometer Bias ($\mathbf{b}_{a\,y}$) (f) Accelerometer Bias ($\mathbf{b}_{a\,z}$)

(g) Velocity ($\mathbf{v}_x$) (h) Velocity ($\mathbf{v}_y$) (i) Velocity ($\mathbf{v}_z$)

Figure 8. Vario X-Treme VD vs GPS Estimation Errors (solid line) and Estimated Error Standard Deviation (dashed line)

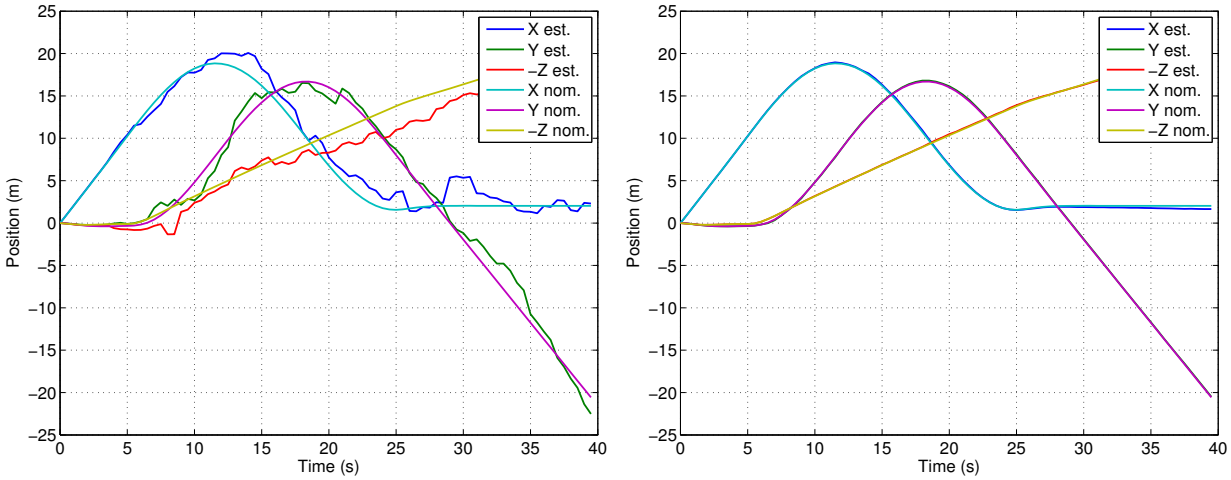

(a) GPS Aiding (b) Vario X-Treme Model Aiding

Figure 9. Trajectory Estimation for the Vario X-Treme

C. LASER Aiding

The LASER range sensor implementation is analyzed for a landing operation of an air vehicle equipped with a standard GPS/INS unit. The vehicle hovers the landing zone and activates the LASER at $t = 30$ s to acquire the ground height and enhance the distance-to-ground estimate. The actual terrain height is $h_S = 4$ m, the filter estimate is $\hat{h}_S = 0$ m and the estimated error variance of $\hat{h}_S$ is set at 16 m^2.

As depicted in Figure 10, using solely the GPS sensor yields high uncertainty on the position estimate, which may render landing unfeasible. The LASER range finder successfully estimates the ground height and improves significantly the velocity and position estimates accuracy along the z axis.

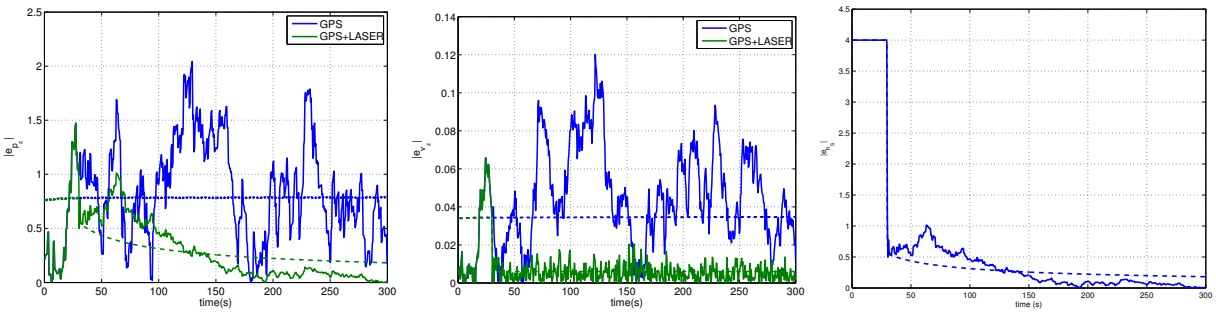

(a) Position ($\mathbf{p}_z$) (b) Velocity ($\mathbf{v}_z$) (c) Ground Height (h_S)

Figure 10. LASER Aiding Estimation Errors (solid line) and Estimated Error Standard Deviation (dashed line)

VII. Conclusion

A new embedded methodology to integrate the vehicle dynamics in the navigation system was successfully implemented. The internal VD system accuracy was shown to be equivalent to the classical external vehicle model architecture, while computational savings were obtained by introducing the INS states in the vehicle dynamics. The application of the proposed technique to a highly nonlinear Vario X-Treme helicopter model validated the approach towards practical applications.

Trimming trajectory simulation results show that the bias calibration errors are quickly compensated and that bias estimates are enhanced. The linear and angular velocity are also drastically improved in

comparison to the classical GPS/INS configuration. Position and attitude errors, although not observable by the VD model, remain bounded for long periods of time. Therefore, the internal VD architecture arises as a valuable software based aiding source for navigation systems.

Together with the LASER range finder sensor, that provides high precision altitude readings for the critical takeoff and landing maneuvers, the proposed techniques are found suited for performing autonomous missions with limited GPS availability and/or high accuracy positioning requirements.

Further work will focus on the observability of the overall navigation system and on a method to analytically identify the contribution of the vehicle model to the state observability. Using specific and under research techniques to tune the navigation system's vehicle model, the proposed aiding architecture will be implemented on a navigation system for the Vario X-Treme model-scale helicopter,[22] property of the Institute for Systems and Robotics.

Acknowledgments

The authors would like to thank to Bruno Guerreiro e Rita Cunha from ISR/IST for their valuable contribution to the development of the helicopter simplified dynamic model used in the paper.

This work was partially supported by Fundação para a Ciência e a Tecnologia (ISR/IST plurianual funding) through the POS_Conhecimento Program that includes FEDER funds and by the POSI/SRI/41938/2001 ALTICOPTER project. The work of J.F. Vasconcelos was supported by a PhD Student Scholarship, SFRH/BD/18954/2004, from the Portuguese FCT POCTI programme.

A. Helicopter Model Summary

This Section briefly describes the nonlinear Vario X-Treme helicopter model presented in Ref. 22, and simplified under the assumptions described in Ref. 23. The motion of the helicopter is described using the rigid body equations of motion

$$\dot{\boldsymbol{\omega}} = \mathbf{I}_B^{-1}\left(\mathbf{n}\left(\boldsymbol{\omega},\mathbf{u},\mathbf{u}_{hc}\right) - \boldsymbol{\omega}\times\mathbf{I}_B\,\boldsymbol{\omega}\right) \tag{48}$$

$$\dot{\mathbf{u}} = -\boldsymbol{\omega}\times\mathbf{u} + \frac{1}{m}\mathbf{f}\left(\boldsymbol{\omega},\mathbf{u},\mathbf{u}_{hc}\right) + \mathcal{R}'^{\,E}\mathbf{g} \tag{49}$$

$$\dot{\mathcal{R}} = \mathcal{R}\left[\boldsymbol{\omega}\times\right] \tag{50}$$

where m is the vehicle mass, $\mathbf{I}_B$ is the tensor of inertia about the Center of Mass coordinate frame, denoted by $\{G\}$, $\mathbf{u}_{hc}$ is the helicopter command vector and $\mathbf{f}$ and $\mathbf{n}$ are the vectors of external forces and moments, respectively, along the same frame.

The input vector $\mathbf{u}_{hc} = \begin{bmatrix}\theta_{c_0} & \theta_{c_{1c}} & \theta_{c_{1s}} & \theta_{c_{0_t}}\end{bmatrix}'$ comprises the blade pitch angle commands for the main rotor collective θ_{c_0}, main rotor longitudinal cyclic $\theta_{c_{1c}}$, main rotor lateral cyclic $\theta_{c_{1s}}$ and the tail rotor collective $\theta_{c_{0_t}}$. To compensate the shape of the rotor, θ_{c_0} and $\theta_{c_{0_t}}$ swashplate inputs are corrected in the helicopter model using the intermediate variables $\theta_0 = \theta_{c_0} + \alpha_0$ and $\theta_{0_t} = \theta_{c_{0_t}} + \alpha_{0_t}$, where α_0 and α_{0_t} are the lift curve slope offsets for the main and tail rotor blades, respectively.

In helicopters equipped with the Bell-Hiller mechanism,[22] the cyclic blade pitch angles result from the combination of the commands introduced by the swashplate and the flybar flapping. The blade pitch dynamics are described by

$$\dot{\theta}_{1c} = C_{\theta_1}\,\theta_{1c} + C_{\theta_3}\,\theta_{c_{1c}} \tag{51}$$

$$\dot{\theta}_{1s} = C_{\theta_1}\,\theta_{1s} + C_{\theta_3}\,\theta_{c_{1s}} + C_{\theta_8}\,\mu\,\lambda_0 \tag{52}$$

with the state coefficients given by

$$C_{\theta_1} = -\frac{\Omega\,\gamma_f}{4\left[\left(\frac{\gamma_f}{8}\right)^2+4\right]}\,,\quad C_{\theta_3} = \frac{\Omega\,(c_4+c_1)\,\gamma_f}{4c_2\left[\left(\frac{\gamma_f}{8}\right)^2+4\right]}\,,\quad C_{\theta_8} = -\frac{\eta_2\,\Omega\,\gamma_f}{2c_2\left[\left(\frac{\gamma_f}{8}\right)^2+4\right]} \tag{53}$$

where μ is the normalized forward velocity at the main rotor, λ_0 is the normalized collective downwash induced by main rotor, Ω is the main rotor angular speed, γ_f is the flybar Lock number, and c_1, c_2 and c_4 are flybar pitching parameters.

For smooth low velocity maneuvers, the effects of the fuselage, horizontal tailplane and vertical fin on the body dynamics are negligible. The total force and moment vectors are modeled accounting for the main rotor and tail rotor components, which are dominant over the remaining terms, yielding

$$\begin{aligned} \mathbf{f} &= \mathbf{f}_{mr} + \mathbf{f}_{tr} && (54)\\ \mathbf{n} &= \mathbf{n}_{mr} + \mathbf{n}_{tr} && (55) \end{aligned}$$

where mr stands for main rotor and tr for tail rotor.

The main rotor is the primary source of lift required to sustain the helicopter, and generates other forces and moments that allow for the control of the helicopter position, orientation and velocity. The main forces and moments are described by

$$\mathbf{f}_{mr} := \begin{bmatrix} X_{mr} \\ Y_{mr} \\ Z_{mr} \end{bmatrix} = -s_1 \begin{bmatrix} a_0 \left(\frac{1}{2}\,\theta_{1s}\,\lambda_0 + \mu\,\lambda_0\,\theta_0\right) + \delta_0\,\mu \\ a_0 \left(\frac{1}{2}\,\theta_{1c}\,\lambda_0\right) \\ a_0 \left(\frac{2}{3}\,\theta_0 - \lambda_0\right) \end{bmatrix} \quad (56)$$

$$\mathbf{n}_{mr} = \begin{bmatrix} -k_\beta\,\beta_{1s} \\ -k_\beta\,\beta_{1c} \\ \frac{1}{2}\,s_2\,\delta_0 + s_2\,a_0 \left(\frac{2}{3}\,\theta_0\,\lambda_0 - \lambda_0^2\right) \end{bmatrix} + \begin{bmatrix} Y_{mr}\,h_R \\ -X_{mr}\,h_R + Z_{mr}\,x_{cm} \\ -Y_{mr}\,x_{cm} \end{bmatrix} \quad (57)$$

where s_1 and s_2 are the main rotor's force and moment normalizing constants, a_0 is the lift curve slope for the main rotor, δ_0 is the main rotor profile drag coefficient, k_β is the center-spring rotor stiffness, and x_{cm} and h_R determine the position of the main rotor hub aft and above the center of mass, respectively.

The flapping motion is described by the blade flap angle vector $\boldsymbol{\beta} = \begin{bmatrix} \beta_0 & \beta_{1c} & \beta_{1s} \end{bmatrix}$, where β_0 denotes the collective mode, and β_{1c} and β_{1s} represent the longitudinal and lateral cyclic modes, respectively. The blade flapping dynamic can be approximated by the steady-state solution given by

$$\begin{aligned} \beta_0 &= C_{\beta_1}\,\theta_0 && (58)\\ \beta_{1c} &= C_{\beta_3}\,\mu\,\theta_0 + C_{\beta_4}\,\theta_{1c} - C_{\beta_5}\,\theta_{1s} + C_{\beta_6}\,\omega_x + C_{\beta_7}\,\omega_y + C_{\beta_8}\,\mu\,\lambda_0 - C_{\beta_4}\,\lambda_{1c} && (59)\\ \beta_{1s} &= C_{\beta_9}\,\mu\,\theta_0 + C_{\beta_5}\,\theta_{1c} + C_{\beta_4}\,\theta_{1s} + C_{\beta_7}\,\omega_x - C_{\beta_6}\,\omega_y + C_{\beta_{10}}\,\mu\,\lambda_0 - C_{\beta_5}\,\lambda_{1c} && (60) \end{aligned}$$

with the state coefficients

$$\begin{aligned} C_{\beta_1} &= \frac{\frac{\gamma}{8}}{\frac{\gamma}{8} S_\beta + 1}\,, \quad C_{\beta_3} = -\frac{\frac{8}{3}}{S_\beta^2 + 1}\,, \quad C_{\beta_4} = \frac{S_\beta}{S_\beta^2 + 1}\,, \quad C_{\beta_5} = \frac{1}{S_\beta^2 + 1}\,, \quad C_{\beta_6} = \frac{16}{\Omega\,\gamma}\,\frac{S_\beta}{S_\beta^2 + 1} \\ C_{\beta_7} &= \frac{16}{\Omega\,\gamma}\,\frac{1}{S_\beta^2 + 1}\,, \quad C_{\beta_8} = \frac{2}{S_\beta^2 + 1}\,, \quad C_{\beta_9} = \frac{\frac{8}{3}\,S_\beta}{S_\beta^2 + 1}\,, \quad C_{\beta_{10}} = -\frac{2\,S_\beta}{S_\beta^2 + 1} \end{aligned} \quad (61)$$

where the longitudinal cyclic induced downwash and forward normalized velocity are described by

$$\lambda_{1c} = \begin{cases} 0 & ,\mu = 0\,(\text{vertical flight}) \\ \lambda_0 \left(\sqrt{1 + \left(\frac{\lambda_0}{\mu}\right)^2} - \left|\frac{\lambda_0}{\mu}\right| \right) & ,\text{otherwise} \end{cases} \quad (62)$$

$$\mu = \frac{u_x - h_R \omega_y}{\Omega R_m} \quad (63)$$

the lateral cyclic downwash is neglected $\lambda_{1s} = 0$, S_β is the blade stiffness number, R_m is the main rotor radius and γ is the Lock number.

The tail rotor whose main role is to counteract the main rotor torque, produces the following force and torque

$$\mathbf{f}_{tr} := \begin{bmatrix} X_{tr} \\ Y_{tr} \\ Z_{tr} \end{bmatrix} = s_{1_t}\,a_{0_t} \begin{bmatrix} 0 \\ \frac{2}{3}\,\theta_{0_t} - \lambda_{0_t} \\ 0 \end{bmatrix} \quad (64)$$

$$\mathbf{n}_{tr} = \begin{bmatrix} Y_{tr}\,h_{tr} \\ -\frac{1}{2}\,s_{2_t}\,\delta_{0_t} - s_{2_t}\,a_{0_t} \left(\frac{2}{3}\,\theta_{0_t}\,\lambda_{0_t} - \lambda_{0_t}^2\right) \\ -Y_{tr}\,(x_{cm} + l_{tr}) \end{bmatrix} \quad (65)$$

where λ_{0_t} is the collective induced downwash of the tail rotor, s_{1_t} and s_{2_t} are the tail rotor's force and moment normalizing constants, a_{0_t} is the tail rotor lift curve slope, δ_{0_t} is the tail rotor profile drag coefficient, l_{tr} is the distance from the tail rotor hub to the fuselage reference point and h_{tr} is the height of tail rotor hub above the fuselage reference point.

The collective induced downwash at the main and tail rotors are given by

$$\lambda_0 = -\frac{a_0\, s}{16} + \sqrt{\left(\frac{a_0\, s}{16}\right)^2 + \frac{a_0\, s}{12}\,\theta_0}\,, \quad \lambda_{0_t} = -\frac{a_{0_t}\, s_t}{16} + \sqrt{\left(\frac{a_{0_t}\, s_t}{16}\right)^2 + \frac{a_{0_t}\, s_t}{12}\,\theta_{0_t}} \tag{66}$$

where s and s_t are the main and tail rotor's solidity, respectively.

References

[1]Savage, P., "Strapdown Inertial Navigation Integration Algorithm Design Part 1: Attitude Algorithms," *AIAA Journal of Guidance, Control, and Dynamics*, Vol. 21, No. 1, January-February 1998, pp. 19–28.

[2]Savage, P., "Strapdown Inertial Navigation Integration Algorithm Design Part 2: Velocity and Position Algorithms," *AIAA Journal of Guidance, Control, and Dynamics*, Vol. 21, No. 2, March-April 1998, pp. 208–221.

[3]Ignagni, M., "Duality of Optimal Strapdown Sculling and Coning Compensation Algorithms," *Journal of the Institute of Navigation*, Vol. 45, No. 2, Summer 1998, pp. 85–95.

[4]Roscoe, K., "Equivalency Between Strapdown Inertial Navigation Coning and Sculling Integrals/Algorithms," *AIAA Journal of Guidance, Control, and Dynamics*, Vol. 24, No. 2, 2001, pp. 201–205.

[5]Vasconcelos, J., Oliveira, P., and Silvestre, C., "Inertial Navigation System Aided by GPS and Selective Frequency Contents of Vector Measurements," *Proceedings of the AIAA Guidance, Navigation, and Control Conference (GNC2005)*, American Institute for Aeronautics and Astronautics, San Francisco, USA, August 2005.

[6]Bryson, M. and Sukkarieh, S., "Vehicle Model Aided Inertial Navigation for a UAV Using Low-Cost Sensors," *Proceedings of the Australasian Conference on Robotics and Automation*, Canberra, Australia, December 2004.

[7]Bar-Itzhack, I. and Harman, R., "The Effect of Sensor Failure on the Attitude and Rate Estimation of the MAP Space-Craft," *AIAA Guidance, Navigation and Control Conference*, 2003.

[8]Ma, X., Sukkarieh, S., and Kim, J., "Vehicle Model Aided Inertial Navigation," *Proceedings of the IEEE Intelligent Transportation Systems*, Vol. 2, Shangai, China, 2003, pp. 1004–1009.

[9]Gaylor, D., *Integrated GPS/INS Navigation System for Design for Autonomous Spacecraft Rendezvous*, Ph.D. thesis, The Univesity of Texas at Austin, 2003.

[10]Dissanayake, G. and Sukkarieh, S., "The Aiding of a Low-Cost Strapdown Inertial Measurement Unit Using Vehicle Model Constraints for Land Vehicle Applications," *IEEE Transactions On Robotics and Automation*, Vol. 17, No. 5, October 2001, pp. 731–747.

[11]Koifman, M. and Bar-Itzhack, I., "Inertial Navigation System Aided by Aircraft Dynamics," *IEEE Transactions on Control Systems Technology*, Vol. 7, No. 4, July 1999, pp. 487–493.

[12]Goshen-Meskin, D. and Bar-Itzhack, I., "Observability Analysis of Piece-Wise Constant Systems - Part I: Theory," *IEEE Transactions On Aerospace and Electronic Systems*, Vol. 28, No. 4, October 1992, pp. 1056–1067.

[13]Goshen-Meskin, D. and Bar-Itzhack, I., "Observability Analysis of Piece-Wise Constant Systems - Part II: Application to Inertial Navigation In-Flight Alignment," *IEEE Transactions On Aerospace and Electronic Systems*, Vol. 28, No. 4, October 1992, pp. 1068–1075.

[14]Julier, S. and Durrant-Whyte, H., "On The Role of Process Models in Autonomous Land Vehicle Navigation Systems," *IEEE Transactions on Robotics and Automation*, Vol. 19, No. 1, February 2003, pp. 1–13.

[15]Brown, R. and Hwang, P., *Introduction to Random Signals and Applied Kalman Filtering*, John Wiley & Sons, Inc., 3rd ed., 1997.

[16]Britting, K., *Inertial Navigation Systems Analysis*, John Wiley & Sons, Inc., 1971.

[17]Markley, F., "Attitude Error Representations for Kalman Filtering," *AIAA Journal of Guidance, Control, and Dynamics*, Vol. 26, No. 2, March-April 2003, pp. 311–317.

[18]Pittelkau, M., "Rotation Vector in Attitude Estimation," *AIAA Journal of Guidance, Control, and Dynamics*, Vol. 26, No. 6, November-December 2003, pp. 855–860.

[19]Savage, P., *Strapdown Analytics*, Vol. 1, Strapdown Associates, Inc., Maple Plain, MN, 2000.

[20]Craig, J., *Introduction to Robotics*, Addison-Wesley, New York, 2nd ed., 1989.

[21]Gelb, A., *Applied Optimal Estimation*, MIT Press, 1974.

[22]Cunha, R. and Silvestre, C., "Dynamic Modeling and Stability Analysis of Model-Scale Helicopters with Bell-Hiller Stabilizing Bar," *AIAA Guidance, Navigation and Control Conference*, 2003.

[23]Guerreiro, B., "Vario X-Treme Helicopter nonlinear model: Complete and Simplified Expressions," Tech. rep., Institute for Systems and Robotics, 2005.